NASA Contractor Report 3863

Design Study of Technology Requirements for High Performance Single-Propeller-Driven Business Airplanes

David L. Kohlman and James Hammer

CONTRACT NAS1-16363
JANUARY 1985

NASA

NASA Contractor Report 3863

Design Study of Technology Requirements for High Performance Single-Propeller-Driven Business Airplanes

David L. Kohlman and James Hammer
Flight Research Laboratory
University of Kansas Center for Research, Inc.
Lawrence, Kansas

Prepared for
Langley Research Center
under Contract NAS1-16363

National Aeronautics
and Space Administration

**Scientific and Technical
Information Branch**

1985

TABLE OF CONTENTS

TABLE OF CONTENTS (cont'd.)

1. INTRODUCTION

Recent developments in aerodynamic, structural, and propulsion technologies have greatly increased the potential for significant improvements in the performance, fuel efficiency, safety, and utility of general aviation airplanes. The changing environment--social, economic, and technical--in which general aviation airplanes operate has, in addition, greatly increased the motivation to develop and incorporate those technologies so that their full potential for improvement can be realized in production airplanes.

In particular, reduced airline service and rapidly increasing fares have increased the need for improved range, speed, and payload of general aviation aircraft. And as business turns more to general aviation, improved safety levels will be demanded. Finally, the continuing concern for energy conservation and the rapidly rising cost of fuel provide a strong motivation for a significant increase in fuel efficiency.

As costs for the airframe, engines, and fuel have increased dramatically, the single-engine, single-propeller airplane has become very attractive. Not only are its initial cost, maintenance, and fuel consumption lower than for a conventional twin-engine airplane, but also it is not as difficult to fly and as complex to operate as a twin, particularly with an engine failure. The only compromise with safety is the fact that the single-engine airplane must make an emergency landing after engine failure, whereas the twin does have the safety of an additional engine. Nevertheless, accident statistics show that

the fatality rate of single-engine airplanes due to engine failure is actually better than that of twin-engine general aviation airplanes. Another possibility, addressed in this study, is the use of two engines to drive a single propeller, a concept featured in the recently developed Lear Fan twin-turboprop airplane. This concept combines the centerline thrust and good handling qualities of a single-engine configuration with the inherent engine safety of a twin.

The base mission selected for analysis in this study is a range of 1300 nm (no reserves) at 300 knots true airspeed, cruise altitude of 35,000 ft, and a payload of 1200 lb or six persons including crew and baggage. As shown in Figure 1.1 this mission represents almost a 100 percent increase in both range and cruise over current single-engine business airplanes. Indeed, it is comparable to that for current high-performance, twin-engine, turboprop airplanes.

Previous studies (References 1-4) have already demonstrated that these significant improvements in performance can be achieved, along with more than a 100 percent increase in specific range, by the proper combination of current and advanced technologies. The purpose of this study is to identify the individual and synergistic effects of various advanced technologies on the optimization of this class of airplane for fuel efficiency. The General Aviation Synthesis Program (GASP), Reference 5, was used to provide more detailed and accurate mission performance calculations than have previously been obtained. The effects of various combinations of aspect ratio, wing loading, and natural laminar flow were determined, in combination with four different advanced propulsion systems: GATE (General Aviation Turbine Engine).

reciprocating, diesel, and rotary. In addition, the effects of fuselage and wing drag coefficients, various high lift systems, composite structure, canard configuration, and variations in mission range, payload and cruise speed were determined.

A brief preliminary design study was conducted for an electric propulsion airplane capable of performing the base mission. Recent advancements in battery and fuel cell technology, using lithium as an active material, have made this an attractive alternative to consider, although the feasibility is likely to be less certain at this time than any of the advanced petroleum-fueled engines.

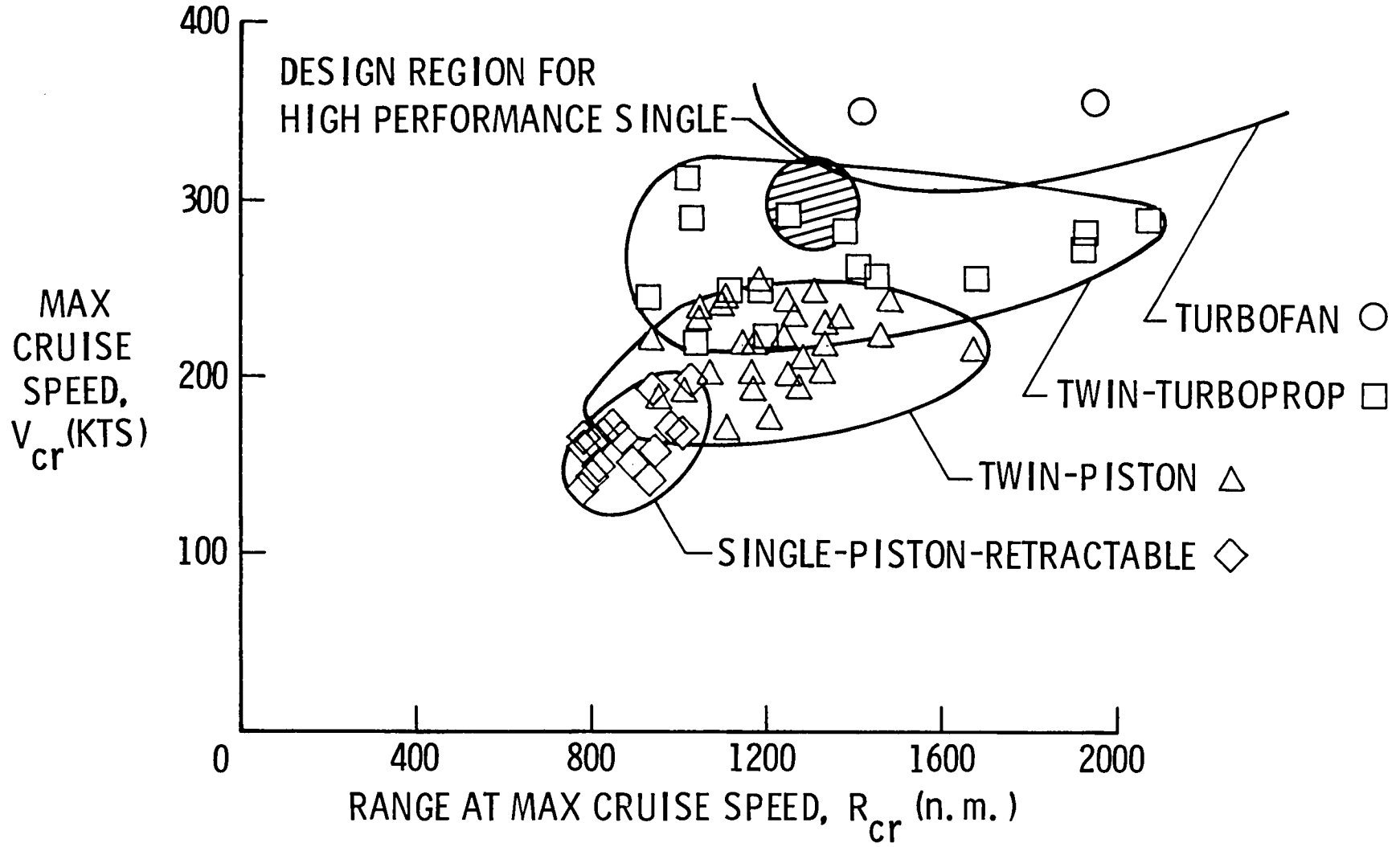

Figure 1.1 Comparison of High-Performance Single Engine Airplane Performance Goal with Current Production Airplane Performance.

2. NOMENCLATURE

AR aspect ratio

BHP brake horsepower

C_d section drag coefficient

C_L lift coefficient

C_ℓ section lift coefficient

h altitude

L/D lift-to-drag ratio

$(L/D)_m$ maximum lift-to-drag ratio

R range

R_c Reynolds number based on chord length

S wing area

V true airspeed

V_m true airspeed for maximum L/D

V_{s_o} equivalent stall airspeed at maximum gross weight in landing configuration

W weight

W_p payload

Subscripts

max maximum

cr cruise

TO takeoff

Acronyms

GASP	General Aviation Synthesis Program
HIPS	High-performance, single-engine airplane
SIR	Spark-ignited, reciprocating engine
FAR	Federal Aviation Regulations
FAA	Federal Aviation Administration
NASA	National Aeronautics and Space Administration

3. BASELINE CONFIGURATION ANALYSIS

3.1 Description of Baseline Configuration

The baseline configuration for the high-performance, single-engine airplane (HIPS) analysis was defined primarily by the baseline mission (Table 3.1) and the choice of engine, wing loading, and aspect ratio.

The Pratt and Whitney PT6A-45A turboprop engine, a currently available model, was chosen as the baseline engine. Its characteristics are summarized in Table 3.2. During parametric studies that sized the airplane to the baseline mission, a rubber engine (same specifics while varying weight and power) was assumed.

Based on previous studies, the baseline configuration was assigned a wing loading of 40 lb/ft^2 and an aspect ratio of 8. The computer program, GASP (Ref. 5), was then used to size the airplane to meet the mission requirements of Table 3.1. The results are presented in Table 3.3.

Other assumptions made in computing the characteristics of the baseline configuration are

- tractor propeller configuration
- turbulent boundary layer on wings and fuselage
- conventional aluminum structure
- single-slotted Fowler flaps, 75% span
- pressurized cabin, 8 psf differential pressure.

The baseline configuration next was changed systematically to determine the effect of aspect ratio, wing loading, wing drag, and fuselage drag on the characteristics and performance of the

Table 3.1 Baseline Mission

Payload	1200 lb (including 200 lb crew)
Range	1300 nm (no reserves)
Cruise speed	298 knots
Cruise altitude	35000 ft
Takeoff distance over a 50 ft obstacle	< 3000 ft

Table 3.2 Characteristics of the PT6A-45A Turboprop Engine

Weight: 0.40 lb/hp

Lapse Rate: See graph below.

Fuel Consumption: Function of true airspeed only.

sfc ∿ lb/shp·hr	V ∿ knots
0.57	0
0.567	100
0.548	200
0.525	300

from PT6A-45A engine specification, with 10 hp pressurization penalty at cruise

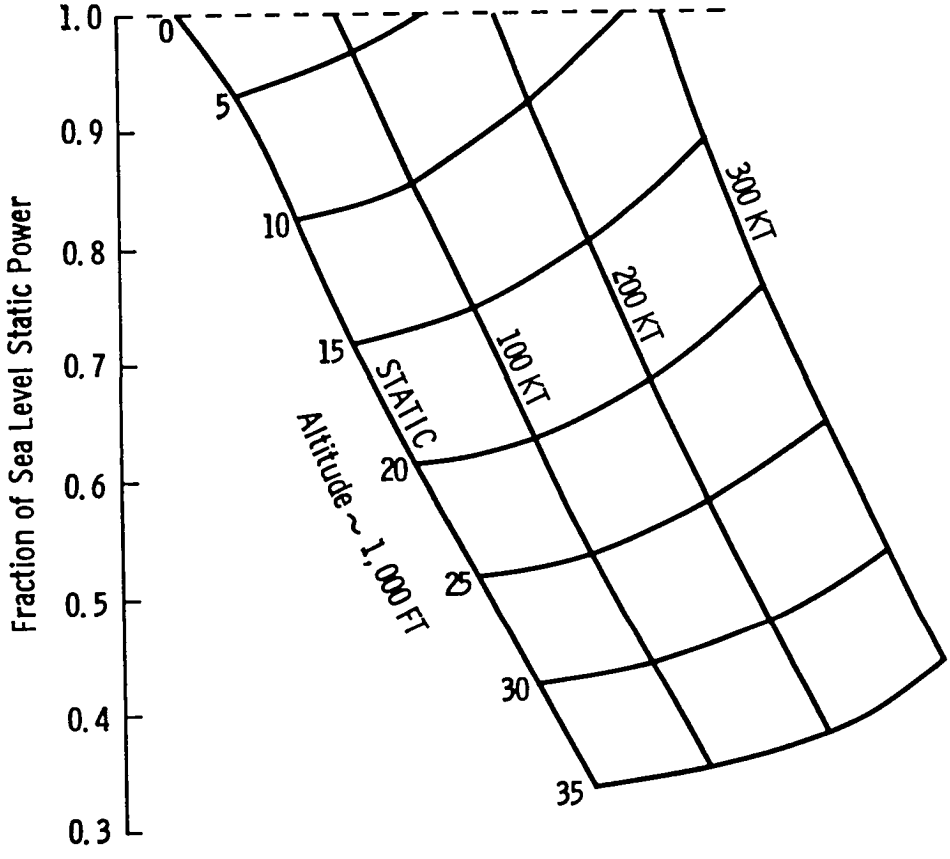

Table 3.3 Description and Performance of the Baseline HIPS Airplane

Configuration Data:	
gross weight	4794 lb
wing area	119.9 ft^2
wing loading	40 psf
aspect ratio	8
wing fuel volume	186.7 gal
empty weight	2669 lb
maximum payload	1200 lb
engine	P&W PT6A-45A
sea level max. power	1289 hp
propulsion system weight	801 lb
Performance:	
cruise speed	298 kt
cruise altitude	35000 ft
range (max. payload)	1300 nm
average cruise specific range	1.63 nm/lb
total fuel for max. payload mission	991 lb
range (max. fuel)	1825 nm
takeoff distance to 50 ft	1879 ft
landing distance from 50 ft	1215 ft
stall speed (takeoff, max. gross weight)	75.9 kt
stall speed (landing, max. gross weight)	64.9 kt
stall speed (landing, end of mission)	58.0 kt

airplane. In all cases, the sizing constraint was that the airplane must be just able to perform the baseline mission in Table 3.1. Throughout this report the cockpit and cabin dimensions were held constant at the values shown in Figure 3.1.

3.2 Effect of Aspect Ratio

Figure 3.2 shows the effect of aspect ratio on gross weight, average cruise specific range, and total mission fuel for various wing loadings. It became apparent early in the program that it was detrimental to reduce the aspect ratio below 8, so the range from 8 to 12 was explored.

In terms of total fuel used and specific range, performance improves as aspect ratio increases even beyond 12, except for the low wing loading of 30 psf. However, it appears that 12 is close to the practical upper limit because wing fuel volume becomes insufficient at the combination of AR = 12 and wing loading of 50 psf; very small tip tanks are required at that point. In addition, improvements in fuel economy and gross weight appear to diminish rapidly as aspect ratio increases beyond 12. Not only does fuel volume become a problem at these high aspect ratios, but space for control system components and flap mechanisms also becomes quite limited.

At the higher wing loadings, increasing the aspect ratio from 8 to 12 results in fuel savings ranging between 6 and 8.5 percent.

3.3 Effect of Wing Loading

Figure 3.3 shows the effect of wing loading on gross weight, average cruise specific range, and total mission fuel for various aspect ratios. The most obvious result is that fuel economy and gross weight are optimized at wing loadings between 45 and 50 psf. High aspect ratios favor slightly higher wing loading.

Of course, as wing loading increases, stall speed increases also. There are certain constraints. Single engine airplanes are currently limited by FAR Part 23 to a maximum stall speed of 61 knots in the landing configuration. This boundary is shown in Figure 3.3. The maximum lift coefficient used to compute this boundary is predicted by GASP to be in the range of 2.8 to 2.9. This is probably somewhat optimistic, even for well designed Fowler flaps, but the possible error in predicted stall speed is not drastic. For the sake of comparison, note that the experimental single-engine Redhawk airplane (Reference 6) with 50% span Fowler flaps and full-span Kruger flaps demonstrated a trimmed $C_{L_{max}}$ of 2.73. The twin-engine ATLIT experimental airplane (Reference 7) with full-span Fowler flaps and no leading edge devices produced a trimmed $C_{L_{max}}$ of 3.03.

Using GASP predictions, stall speed at the optimum wing loading is very close to 70 knots. The 9 knot increase above the FAR 23 constraint allows approximately a 3 percent decrease in gross weight and almost 7 percent increase in fuel efficiency. For a simpler flap system or more conservative $C_{L_{max}}$ predictions, the improvements possible by relaxing the 61 knot rule are much more substantial. When one

realizes that most current single engine airplanes have a wing loading between 17 and 25 psf, it becomes evident that quite substantial gains in fuel economy are still possible with increases in wing loading and cruise altitude.

The primary result of cruising at high altitude and high wing loading is that the cruise L/D is relatively close to maximum L/D at a reasonably high cruise speed. This is illustrated in Figure 3.4. As wing loading is increased, cruise L/D approaches closer to maximum L/D. However, for a given cruise speed, specific range maximizes before L/D at cruise reaches maximum L/D. The reason is that as wing loading increases, maximum L/D decreases because the size of the fuselage relative to the wing increases. So even though one might cruise at $(L/D)_{max}$ with a sufficiently high wing loading, a higher cruise L/D can be achieved with a somewhat lower wing loading.

Of course, one can always decrease the cruise speed of a given configuration until flight at maximum specific range is achieved. If this is done for the baseline configuration, cruise speed is decreased from 298 to 272 knots and average specific range becomes 1.75 nm/lb, a 7.6 percent increase. Range increases to 1410 nm. For this case GASP maximizes specific range at start of cruise rather than cruise L/D. This mission is not flown at $(L/D)_{max}$ because PT6A-45A engine fuel consumption and propeller efficiency are functions of airspeed. Of course, specific range is the preferred parameter to maximize.

The effect of wing loading on approach speed, stall speed, and FAR field length required for landing is shown in Figure 3.5. It is clear that the landing field length required is well under the design target of 3000 ft for all wing loadings investigated[1]. FAR field length is computed by dividing the actual landing distance over a 50 ft obstacle by the factor 0.6. Stall speeds are shown for both maximum gross weight and the weight at the end of the baseline mission.

Wing fuel volume requirements were analyzed and the results are presented in Figure 3.6. As shown, fuel sufficient to accomplish the baseline mission can be carried in the wings for wing loadings below 44 psf (AR = 12) to 48.4 psf (AR = 8). GASP automatically provided tip tanks in computing those cases where wing volume was insufficient, a solution that has been quite acceptable in other production business aircraft.

[1]Throughout this report, wing loading is specified for maximum gross weight unless otherwise stated.

3.4 Effect of Wing Natural Laminar Flow

Recent NASA flight experiments[8,9,10] investigating natural laminar flow phenomena have proven that modern metal or composite general aviation production wing surfaces can be sufficiently free of waviness and roughness to support extensive runs of natural laminar flow. These recent experiments include measurements on the all-composite Bellanca Skyrocket II airplane (Ref. 9). Section drag was determined by wake probe measurements to be $C_d = 0.0047$ at $C_\ell = 0.2$, $R_c = 9.7 \times 10^6$. At $C_\ell = 0.3$, transition was observed to be at the 46 percent chord position on both the upper and lower surfaces. These observations match theoretical predictions well for the NACA 63_2-215 airfoil incorporated on the Skyrocket wing. A typical example of such laminar flow on the Skyrocket wing is shown clearly in Figure 3.7.

Based on these experiences, the present analysis incorporated an NLF(1)-0416 airfoil, a modern natural laminar flow section[11], for the laminar flow trade studies. This airfoil at cruise achieves 40 percent chord upper surface and 50 percent chord lower surface laminar flow at $R_{cr} = 4.0 \times 10^6$. The airfoil was designed for a high section maximum lift capability and achieves $C_{\ell_{max}} = 1.69$ at $R_c = 3.0 \times 10^6$.

The effect on mission performance of natural laminar flow over the wing was studied using GASP. The baseline airplane, which was assumed to have no laminar flow on the wing, was compared with a design using the NLF(1)-0416 airfoil.

The effect of the laminar flow airfoil on drag was input to GASP in a table of two-dimensional airfoil lift vs. drag values. GASP expects the two-dimensional drag values to be input as the ratio of the actual two-dimensional drag to the minimum drag of the same airfoil with completely turbulent flow; i.e., the two-dimensional C_{d_o} for the airfoil under turbulent conditions is taken as 1.0, and C_d values are referred to this number. Input values used for the NLF-0416 are listed in Table 3.4. Drag values are taken from Reference 11.

Table 3.5 compares the baseline and laminar flow airfoil configuration and performance parameters. The total fuel used drops from 946 lb for the baseline to 812 lb for the laminar flow airfoil, approximately a 14% reduction. Gross weight is reduced by 284 lb. The effect of a pusher propeller is discussed in the next section.

In practice, the principle challenge to the practical use of natural laminar flow on this class of airplanes is protection of the aerodynamic surfaces from ice and insect contamination. Developments in porous leading edge ice protection systems[12] offer promise for insect contamination protection as well. Wind tunnel[13] and flight[14] experiments have shown that insect contamination is prevented by keeping the airfoil leading edge region wet.

Future wind tunnel, icing tunnel, and flight experiments by NASA are planned with a porous leading edge configuration illustrated in Figure 3.8. Candidate porous materials for the leading edges include electron or laser beam drilled sheet titanium and porous composite materials. The purpose of these experiments is to validate this ice and insect protection system concept for use on natural laminar flow airfoils.

Table 3.4 Input Drag Values for the NLF(1)-0416 Airfoil

C_ℓ	Two-Dimensional Airfoil C_d/C_{d_o} turbulent
-0.15	0.89
0.15	0.67
0.45	0.61
0.70	0.61
0.95	0.67
1.10	0.89
1.35	1.11
1.55	1.33
1.70	1.89
1.80	2.56

Note: Data from Ref. 11

Table 3.5 Comparison of Baseline Airplane and Baseline with Pusher Propeller, Pusher Propeller and Laminar Flow on Forward Fuselage, and Baseline with NLF 0516 Airfoil

Configuration Data:	Baseline	Pusher Propeller, no fuselage laminar flow	Pusher Propeller and laminar flow on fuselage	NLF(1)-0416 Laminar Wing
gross weight	4794 lb	4727	4680 lb	4510
wing area	119.9 ft^2	118.2	117.0 ft^2	112.8 ft^2
wing loading	40.0 psf	40.0 psf	40.0 psf	40.0 psf
aspect ratio	8	8	8	8
empty weight	2649 lb	2614 lb	2588 lb	2499 lb
sea level max. power	1275 hp	1235 hp	1206 hp	1103 hp
Performance:				
average cruise specific range	1.63 nm/lb	1.69 nm/lb	1.73 nm/lb	1.90 nm/lb
total fuel for max. payload mission (1300 nm range)	946 lb	914 lb	891 lb	812 lb
range (max. fuel)	1823 nm	1853 nm	1874 nm	1952 nm
$(L/D)_{max}$	14.87	15.09	15.26	16.34
$(L/D)_{cruise\ (average)}$	12.96	13.26	13.47	14.29

3.5 Effect of Fuselage Drag

With the conventional single-engine tractor propulsion arrangement, there is a scrubbing drag penalty due to the fuselage being immersed completely in the propwash, resulting in a higher air velocity over the fuselage than if there were no propeller. The unsteady propwash also may eliminate the possibility of achieving laminar flow on the fuselage.

The advantages of a single-engine pusher configuration were investigated using GASP. The effects of scrubbing drag and the achievement of laminar flow were investigated separately.

The increment in fuselage C_{D_f} due to the increase in dynamic pressure behind the propeller is given by:

$$\Delta C_{D_f} = C_{D_f} \left(\frac{q_p}{q} - 1\right) = C_{D_f} \left[\frac{(V + \Delta V)^2}{V^2} - 1\right]$$

$$= C_{D_f} \left[\frac{2V\Delta V}{V^2} + \left(\frac{\Delta V}{V}\right)^2\right]$$

$$\Delta C_{D_f} = 2C_{D_f} \left[\left(\frac{\Delta V}{V}\right) + \frac{1}{2}\left(\frac{\Delta V}{V}\right)^2\right]$$

where:

ΔV = velocity increment due to the propeller

C_{D_f} = fuselage drag coefficient.

q_p = dynamic pressure behind the propeller

ΔV due to the propeller is found by:

$$T = \rho A\left(V + \frac{\Delta V}{2}\right) \Delta V = \rho A\left(V\Delta V + \frac{\Delta V^2}{2}\right)$$

$$T = \rho A V^2 \left(\frac{\Delta V}{V} + \frac{\Delta V^2}{2V^2}\right)$$

$$\left(\frac{\Delta V}{V} + \frac{\Delta V^2}{2V^2}\right) = \frac{T}{\rho A V^2};\ T = D,$$

$$\Delta C_{D_f} = \left[\frac{1}{2} C_D \frac{S}{A}\right] 2C_{D_f} = C_{D_f} C_D \frac{S}{A}$$

$$\frac{\Delta C_{D_f}}{C_D} = C_{D_f} \frac{S}{A}$$

where:

T = thrust, A = propeller disk area, S = wing area.

For the baseline airplane,

$$C_{D_f} = .00787$$

$$S = 119.9 \text{ ft}^2$$

$$A = \pi(3.5 \text{ ft})^2 = 38.48 \text{ ft}^2$$

$$\frac{\Delta C_{D_f}}{C_D} = .00787 \left(\frac{119.9}{38.48}\right) = .025$$

This 2.5% decrease in drag was input to GASP by lowering the value of DELCD, an incremental drag variable, as follows:

Baseline total average cruise $C_D = .0291$

$$\Delta C_D = .0291 \ (-.025) = -.0007$$

Table 3.4 contains values for the resulting configuration and performance parameters. It is seen that by eliminating scrubbing drag alone, the decrease in fuel used for the mission is about 3.4 percent. This reduction exceeds the drag reduction percentage because the airplane is resized to a lower gross weight and wing area.

The effect of partial fuselage laminar flow was also considered. It was assumed that laminar flow extended back to the windshield. The nose section is approximated by GASP as a right circular cone with a length of 6.7 ft and radius of 1.29 ft for the baseline design.

The surface area of the nose cone is 27.7 ft^2. The unit Reynolds number at cruise is 1.24×10^6 ft^{-1}; the Reynolds number for the nose cone is therefore $6.71 \times 1.24 \times 10^6$, or 8.32×10^6.

GASP calculates fuselage profile drag as follows:

$$C_{D_f} = C_{K_f} C_F F(Re) \left(\frac{S}{S_W}\right)$$

where:

C_{D_f} = fuselage drag coefficient

C_{K_f} = fuselage form factor, a function of fuselage length and wetted area

C_F = Mach number dependent skin friction coefficient at a reference Reynolds number of 10^7

$F(Re)$ = Reynolds number correction factor

$\frac{S}{S_W}$ = ratio of fuselage wetted area to wing reference area

For the baseline airplane:

fuselage wetted area $S = 391.5$ ft^2

wing area $S_W = 119.9$ ft^2

$$C_{K_f} = 1.35\left[1 + .0025 \left(\frac{Z_{LF}}{S_{WF}}\right) + 60./(Z_{LF}/S_{WF})^3\right] = 1.253$$

where: Z_{LF} = fuselage length = 32.13 ft

S_{WF} = fuselage diameter at wing = 5.08 ft

C_F = .00283 (from baseline output)

$F(Re) = [\log_{10}(Re_{component})/7]^{-2.6} = .8074$

where: $Re_{component}$ = fuselage Reynolds number = $1.24 \times 10^6 \times 32.13 = 3.98 \times 10^7$

$$C_{D_f} = (1.253)(.00283)(.8074)\left(\frac{391.5}{119.9}\right) = .00935$$

This is the baseline total fuselage drag coefficient based on the wing reference area. To find the change in drag due to laminar flow over the nose, the drag coefficient of the nose section is computed for laminar and turbulent flow:

turbulent:

$$C_{D_N} = C_F F(Re)\left(\frac{S_N}{S_W}\right)$$

where: C_F = .00283

$F(Re) = [\log(1.24 \times 10^6 \times 6.71)/7]^{-2.6} = 1.03$

$$C_{D_N} = (.00283)(1.03)\left(\frac{27.7}{119.9}\right) = .000674$$

laminar:

$$C_{D_N} = \frac{1.328}{\sqrt{Re_N}}\left(\frac{S_N}{S_W}\right)$$

$$C_{D_N} = \frac{1.328}{\sqrt{8.32 \times 10^6}} = \left(\frac{27.7}{119.9}\right) = .000106 \text{ (based on } S_W)$$

The difference between these two drag coefficients, ΔC_{D_N} = .000568, is approximately the overall change in drag coefficient due to laminar flow over the nose. This value is approximate because the turbulent boundary layer skin friction behind the laminar zone is actually changed by the

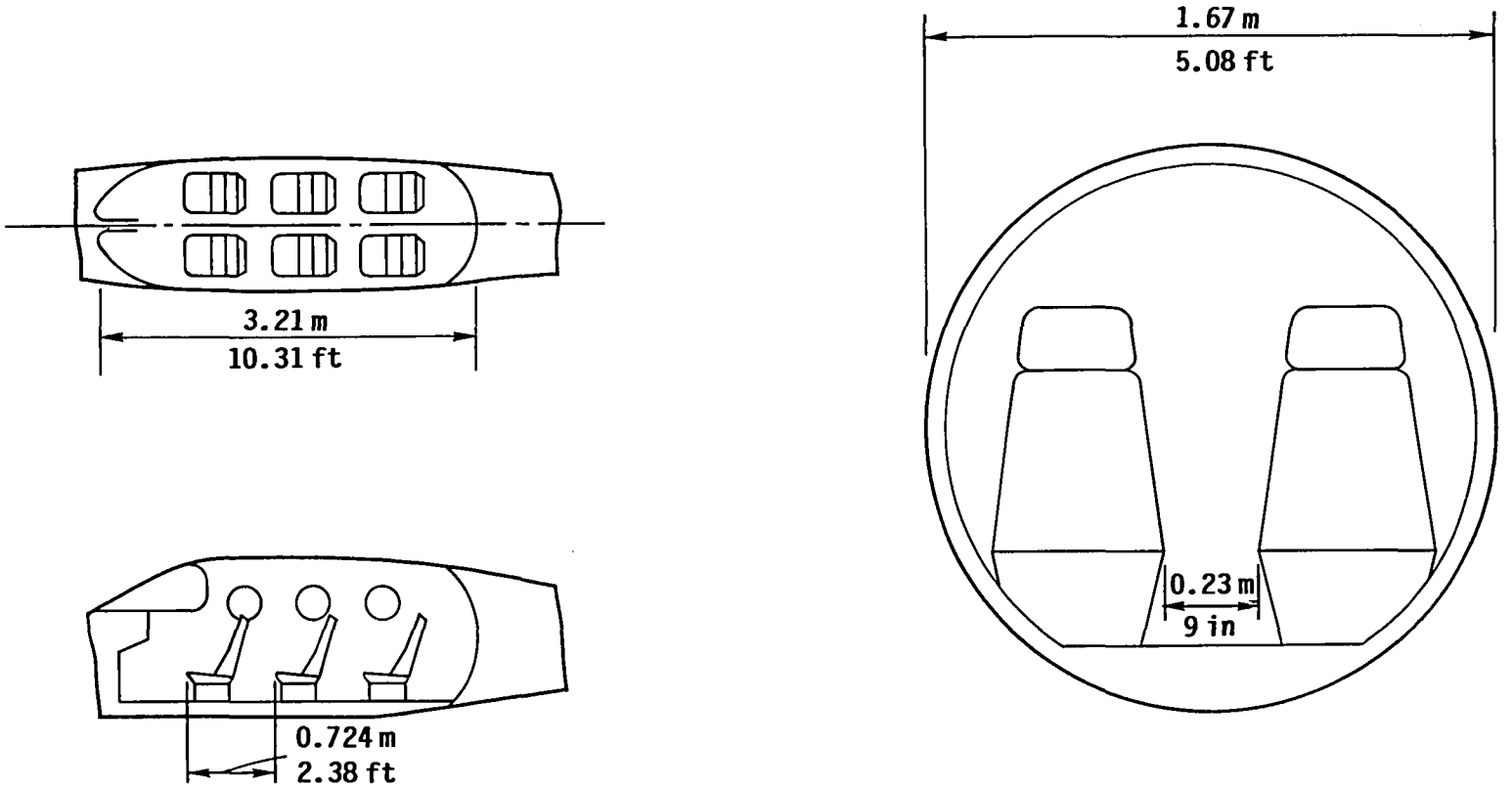

Figure 3.1 Cockpit and Cabin Dimensions for the HIPS Airplane

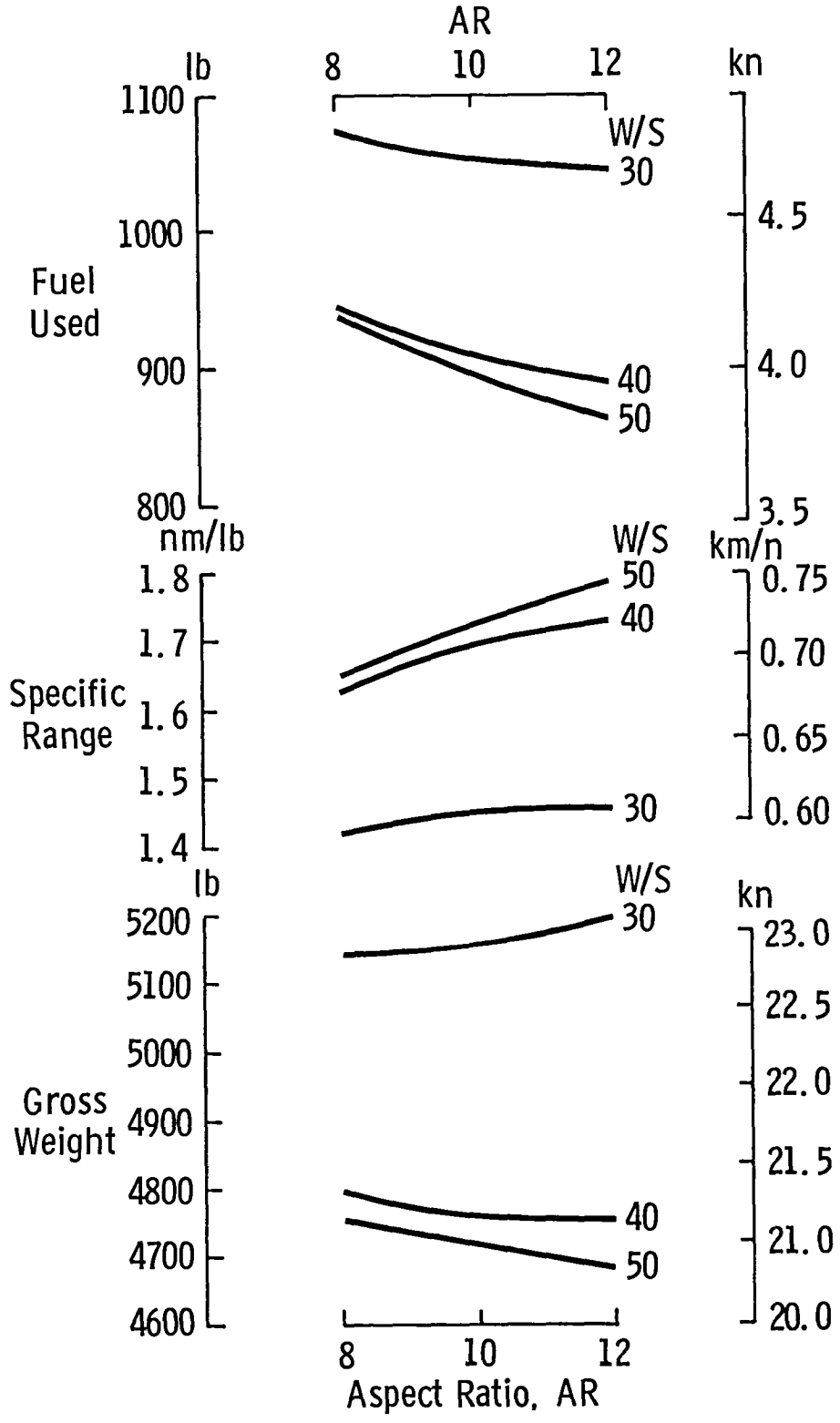

Figure 3.2 Effect of Aspect Ratio on Baseline Airplane

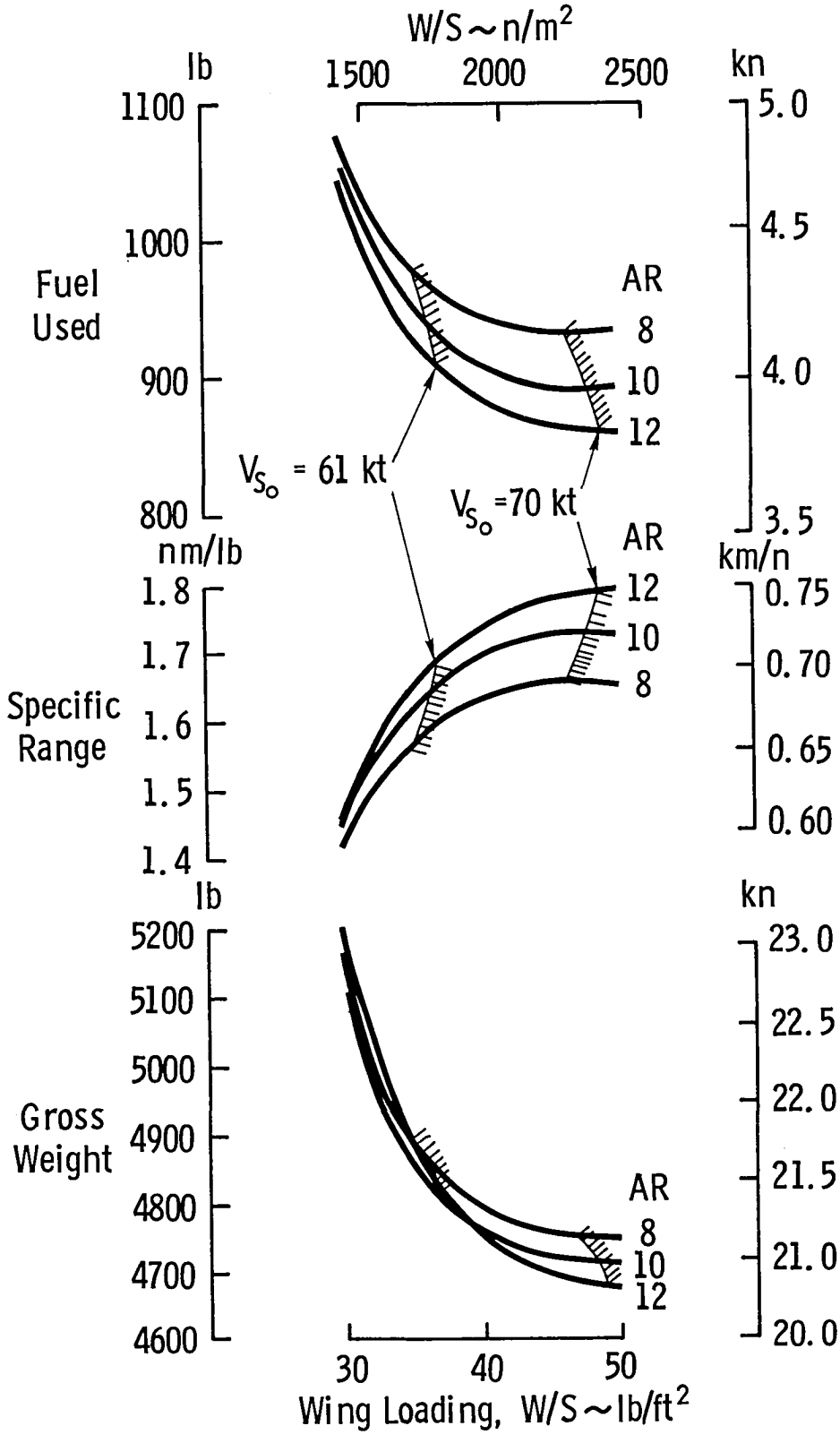

Figure 3.3 Effect of Wing Loading on Baseline Airplane

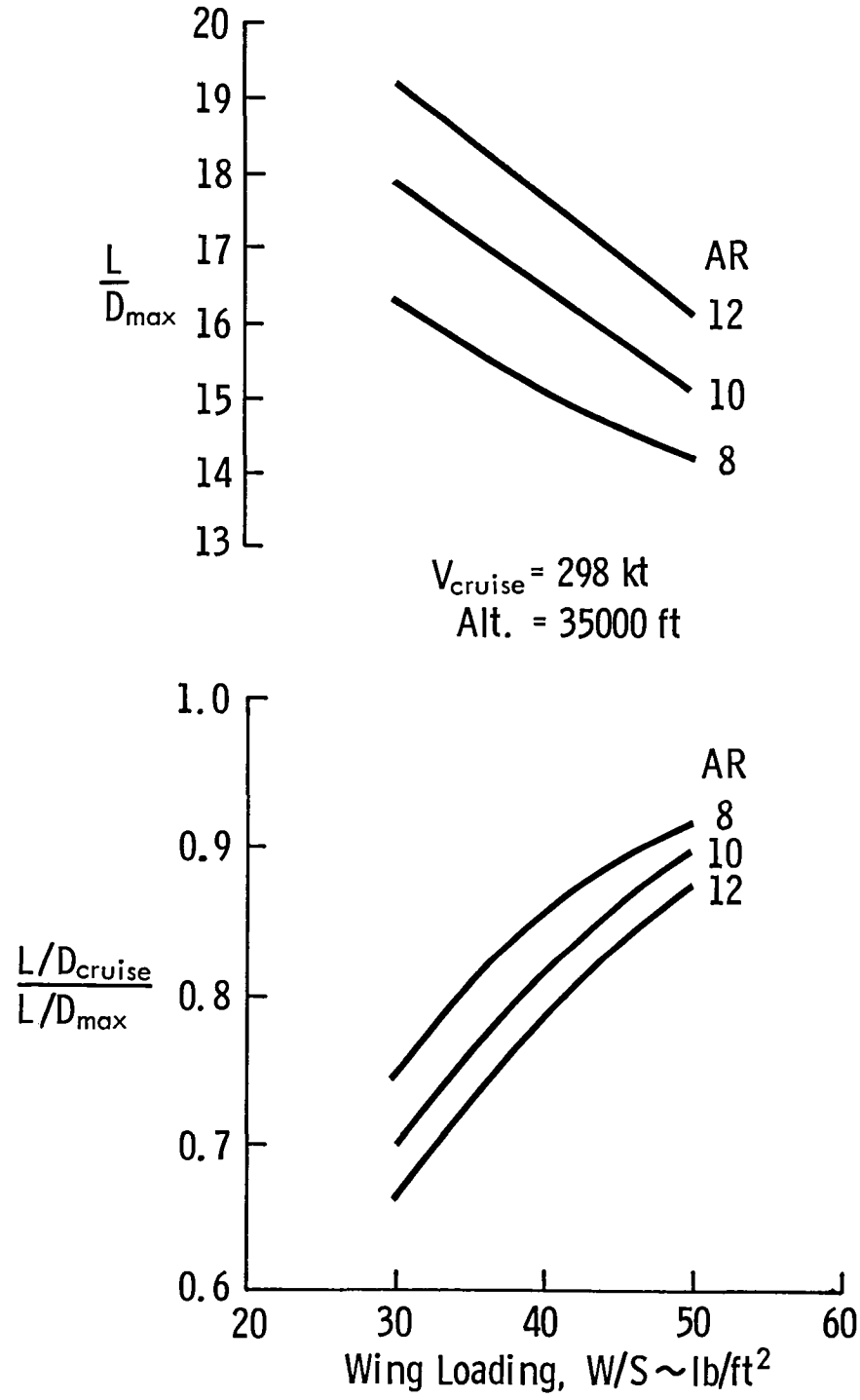

Figure 3.4 Effect of Wing Loading on (L/D) Max and Cruise Matching Parameter of Baseline Airplane

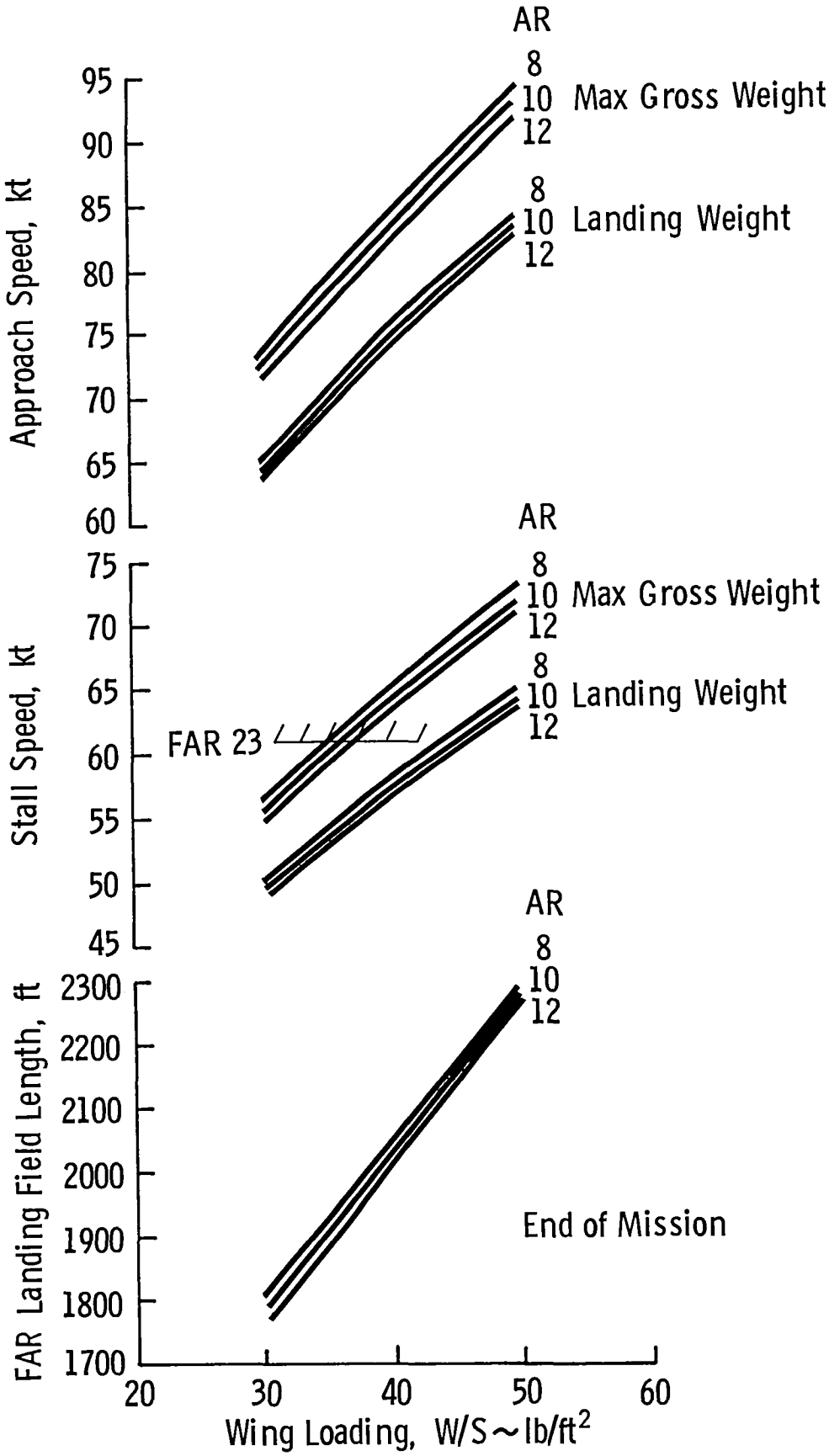

Figure 3.5 Effect of Wing Loading on Approach Speed, Stall and FAR Landing Field Length of Baseline Airplane

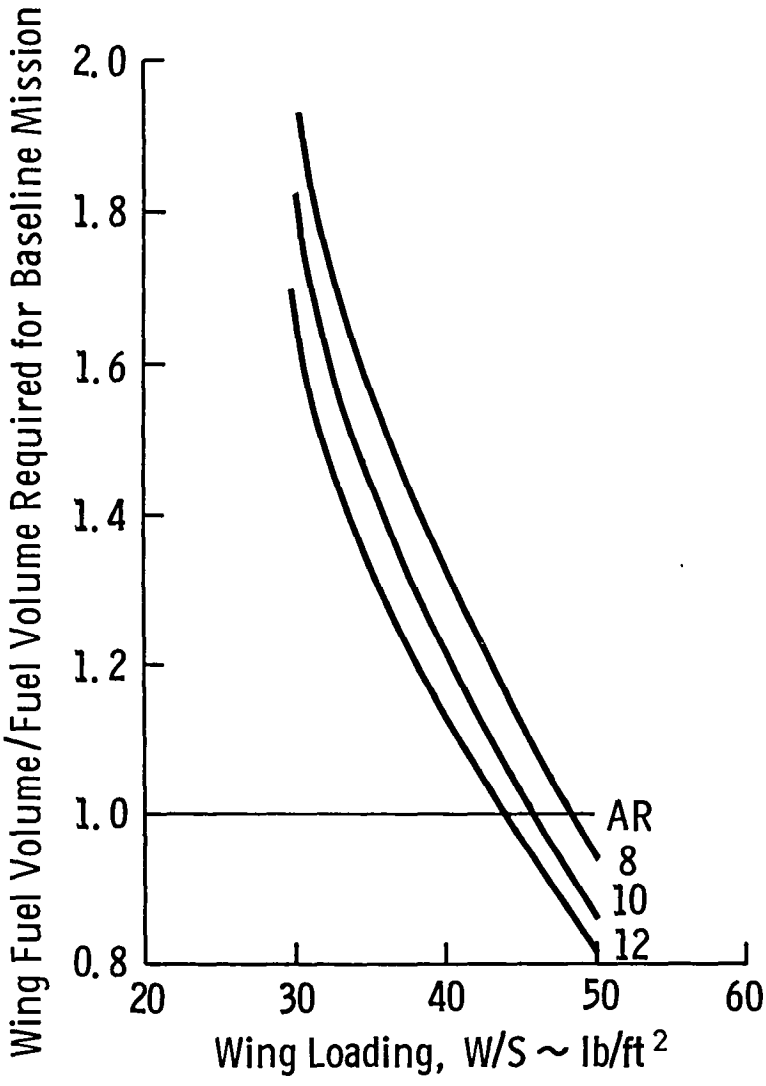

Figure 3.6 Wing Fuel Volume Characteristics of Baseline Airplane

Figure 3.7 Laminar Flow Visualization on the Bellanca Skyrocket II.
$R_x = 1.9 \times 10^6$ ft^{-1}; $C_L = 0.20$ (Reference 9).

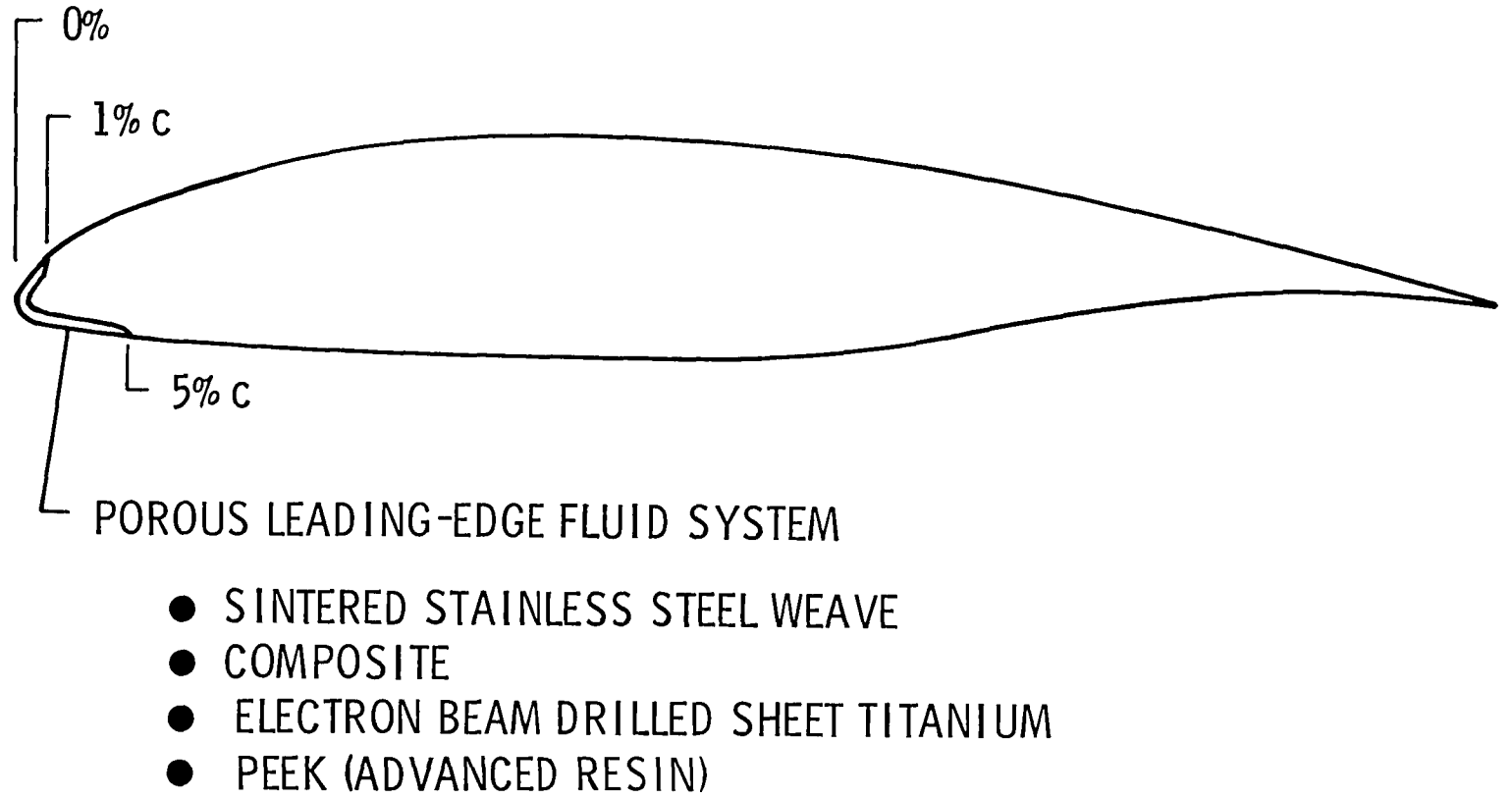

Figure 3.8 Porous Leading Edge Ice and Insect Protection System for Natural Laminar Flow Wings.

4. PROPULSION SYSTEM ANALYSIS

The previous chapter concentrated on the benefits of configuration and aerodynamic optimization. The application of advanced technology to the propulsion system offers the potential for significant improvements in performance and fuel efficiency in comparison with current technology airplanes. These current technology airplanes are represented by the baseline configuration and current production reciprocating engine airplanes.

A considerable amount of research and development effort has been devoted to the field of general aviation propulsion in recent years. The programs have focused on three different approaches: the development of a low-cost turbine engine for general aviation (the GATE program), the evolutionary improvement of the piston engine through advanced materials and design innovations, and developing advanced rotary and diesel engines for use in airplanes.

In this chapter the performance of the HIPS airplane is analyzed using four different advanced technology engines:

1. the low-cost General Aviation Turbine Engine (GATE)
2. a spark-ignited reciprocating engine (SIR)
3. a diesel engine
4. a rotary engine (also known as a Wankel engine)

Characteristics of these engines are presented in detail in the following sections. The performance of the HIPS airplane with each type of engine is then analyzed for various combinations of aspect ratio and wing loading. For the analyses presented in this chapter, it is assumed that the configurations employed a pusher propeller, laminar flow wings, and achieved partial laminar flow on the fuselage.

4.1 GATE Engine

4.1.1 Description of Engine

The General Aviation Turbine Engine (GATE) used for this study is an advanced lightweight turbine with low specific fuel consumption. Figures 4.1, 4.2, and 4.3 show the specific fuel consumption, brake horsepower output, and jet thrust as a function of altitude and airspeed as predicted for GATE design 3013-1. Figure 4.4 shows the scaling of specific fuel consumption with brake horsepower output. Values for altitudes above 25000 ft are extrapolated from the low altitude data. More recent data from NASA Lewis indicate that the design could achieve 10% better fuel consumption and specific weight than indicated by these diagrams. This improvement was added as a simple incremental change by using the GASP program variable SFCPCT to change specific fuel consumption and by changing the engine specific weight constant SWSLS.

The weight equation for this engine with the 10% improvement is:

$$W = \{[(\frac{BHP_{TO}}{494})^{.72} (195)] + 196\} (.9) \qquad (1b)$$

When computing engine weight, the BHP_{TO} value is adjusted for the constant 10 hp pressurization and cabin cooling requirement in cruise by adding $\frac{10 \text{ hp}}{(\text{hp lapse})}$, where (hp lapse) is the fraction of sea level horsepower available at cruise altitude. The (hp lapse) value for this engine at 35000 ft is 0.396.

The GATE power plant was optimized for low cost, with some improvement in specific fuel consumption over current turboprops.

Thus, it does not represent the same high level of technology risk as incorporated in the advanced technology SIR, rotary, and diesel engines.

4.1.2 GASP Engine Routine

An equation derived by a curve fit is used to approximate the dependence of horsepower output on aircraft velocity:

$$\frac{SHP}{SHP_{TO}} = \frac{SHP}{SHP_{TO}}\Big|_{TAS=0} + 3.499 \times 10^{-7}(V)^{2.12} + 0.000173(V)$$

where:

SHP = shaft horsepower

SHP_{TO} = takeoff horsepower

V = true airspeed, knots

The maximum horsepower output at zero airspeed as a function of altitude is found by interpolation from Table 4.1.

Table 4.1 Altitude Lapse Rate for GATE Engine, V = 0

Altitude, 1000 ft	0	10	18	25	30	35
SHP/SHP_{TO}	.609	0.538	0.46	0.377	0.33	0.283

Jet thrust is modeled by three equations, depending on speed:

$$V < 180 \text{ kt}: \quad \frac{\text{Jet Thrust}}{SHP} = 0.158 - 0.000325\ (V)$$

$$180 \leq V < 250 \text{ kt}: \quad \frac{\text{Jet Thrust}}{SHP} = 0.128$$

$$V \geq 250 \text{ kt}: \quad \frac{\text{Jet Thrust}}{SHP} = 0.142 - 0.00038\ (V - 250)$$

The jet thrust equations above take into account the altitudes where these speeds occur in the typical flight profile. Takeoff and initial climb occur at less than 180 kt, and low-altitude climb to cruise occurs between 180 and 250 kt; cruise occurs at more than 250 kt, at 35000 ft.

Specific fuel consumption for the GATE engine is mainly a function of airspeed and the size of the engine and is modeled by two equations:

$$(sfc)' = 0.532 - 0.00038\ (V - 250)$$

$$sfc = (sfc)'\ (2.2187)\ (HP_{TO})^{-.1236}$$

where:

sfc = specific fuel consumption, lb/bhp/hr

V = true airspeed in knots

HP_{TO} = maximum takeoff horsepower

Table 4.2 summarizes the GATE engine characteristics used in this study.

Table 4.2 GATE Engine Summary

Design Features

- Low-cost GATE technology (40% cost reduction)
- 12:1 pressure ratio
- Turbine inlet temperature: 2140°F (cruise)
- Low-cost digital electronic fuel control
- Laminated, radial flow high pressure turbine

Weight and Power

$$\text{Weight: } W = \left[\left(\frac{(BHP_{TO} + \frac{10}{.34})^{.72}}{494}\right) (195) + 196\right] (.9)$$

where: W = weight of engine + accessories, lb

BHP_{TO} = takeoff brake horsepower

Power: See Figure 4.2 for power vs. altitude and airspeed.

Example: Baseline airplane wing planform with pusher engine, laminar wing and fuselage.
Cruise power = 319 hp (298 kt at 35,000 ft).
BHP_{TO} = 806 hp (Figure 4.2)
Engine weight = 433 lb.

Fuel Consumption

See Figure 4.1 for fuel consumption vs. altitude and Mach no.

4.2 Very Advanced Reciprocating Engine (Spark Ignited), (SIR)

This engine is a horizontally opposed, air-cooled engine which operates at a higher rpm than current engines. Advanced turbocharging gives it a lower lapse rate with altitude than the other three engines studied. It is turbocompounded; that is, energy from the exhaust turbine is fed back to the power output shaft through gearing. Stratified charge is employed to reduce fuel consumption and provide multifuel capability (Reference 15). Titanium is used extensively (up to 30% of total weight, excluding accessories). Along with reductions in the weight of other materials, a 30% total weight reduction is achieved over current engines. Continued reductions in the price of aircraft titanium can make this engine cost competitive with the other types of advanced engines.

Cooling drag for the SIR was assumed to be 3.5 percent of the total baseline airplane drag (Reference 3), where the baseline is the PT6-powered conventional configuration with an aspect ratio of 8 and a wing loading of 40 psf. This assumes a considerable improvement in cooling drag over current installations, which may have cooling drag ranging from 5 to 27% of total aircraft drag (Reference 15). The cooling arrangement of this design is very similar to current aircraft engines; the expected cooling drag improvement will be the result of more efficient engine cowling.

Table 4.3 summarizes the characteristics of this engine design. A 10 horsepower pressurization and air conditioning penalty is added to the weight equation by adding $\frac{10 \text{ hp}}{(\text{hp lapse})}$ to the sea level takeoff

horsepower value, where (hp lapse) is the fraction of sea level power available at cruise altitude. The (hp lapse) value for this engine is 0.651 at 35000 ft.

Table 4.3 Very Advanced Spark Ignited Engine Summary

Design Features

- Stratified charge
- Multifuel capability
- Very advanced turbocharging
- Turbocompounded
- Substantial use of titanium
- Horizontally opposed
- Air cooled

Weight and Power

Weight: $W = \left[\frac{\left(BHP_{TO} + \frac{10}{.651}\right)^{.816}}{350} (405) + 121\right]$ (lb)

Power:

Altitude (feet)	Power available as fraction of sea level maximum	
	Maximum Continuous	Continuous Cruise
0	1.0	0.651
5K	1.04	0.694
10K	1.05	0.72
15K	1.029	0.734
20K	0.98	0.729
25K	0.903	0.714
30K	0.80	0.686
35K	0.70	0.651

Example: Baseline airplane aspect ratio and wing loading with pusher engine, laminar wing and fuselage.
Cruise power = 375 hp (298 kt at 35,000 ft).
BHP_{TO} = 576 hp.
Engine weight = 742 lb.

Fuel Consumption

Altitude (feet)	Specific Fuel Consumption lb/bhp/hr	
	Maximum Continous	Cruise
0 to 35K	.334	.331

4.3 Very Advanced Diesel Engine

The high risk diesel engine concept used for this study is represented by a two-stroke cycle radial engine that employs several advanced technologies. It is a scaled version of an engine design studied by NASA Lewis Research Center (Reference 16).

A problem normally associated with diesels is the very high compression ratios that are required only for acceptable starting performance. This problem is eliminated by providing an independent turbocharger loop with a compressor, turbine, and burner. Although cost and complexity are increased, there are some significant design improvements. The starting problems (cold, hot, and restart) associated with diesels are eliminated by starting the turbocharger loop first, then supplying hot pressurized air to start the diesel cylinders. This allows the engine to be designed for a much lower compression ratio (on the order of 10:1), resulting in lower stresses and significant reductions in engine weight. Furthermore, the independent turbocharger loop has ducting which allows the airflow to bypass the diesel; thus, it can provide auxiliary power on the ground without the necessity of starting the entire engine.

The two-stroke diesel cycle provides a high power-to-weight ratio, and complexity is reduced by the elimination of valves. The result is an engine with much less weight for a given sea level power rating than the very advanced SIR engine. Unfortunately, the high lapse rate of the diesel at cruise altitude of 35,000 ft more than offsets this advantage.

The development of advanced turbocharger capability well beyond current performance levels is necessary for a successful diesel design. With the high turbocharger pressure ratio, the engine exhaust air does not contain sufficient energy to power the turbocharger above 17,000 feet altitude. Thus to eliminate an unacceptable thrust lapse at high altitudes, it is necessary to burn fuel in the turbocharger loop to add additional energy to the turbine inlet air. The penalty to specific fuel consumption was accounted for in the data shown in Table 4.4.

The cylinder liners and piston tops are made of ceramic materials to allow the cylinders to run uncooled (adiabatic). This reduces cooling drag and increases engine efficiency by eliminating the heat losses to the cooling airflow. An oil cooler will be required, and some cooling air will be needed for the injectors. Cooling drag for this engine was assumed to 3.5% of the total baseline airplane drag, equal to that required for the very advanced spark ignited engine.

Table 4.4 summarizes the characteristics of the very advanced diesel engine used for this study. The weight equation accounts for the 10 hp requirement for pressurization and cabin cooling at 35,000 ft. The specific fuel consumption is based on total horsepower delivered, including the 10 hp pressurization requirement.

Table 4.4 Very Advanced Diesel Engine Summary

Design Features

- Radial, air cooled
- Two-stroke cycle
- Highly turbocharged
- Catalytic combustor in turbocharger loop for starting and high altitude operation
- Synthetic oil (high engine temperature)
- 65% cooling drag reduction
- Ceramic piston top and cylinder walls

Weight and Power

Weight: $W = 11.879[BHP_{TO} + 30]^{.581} + 121$ (lb)

Power:

Altitude (feet)	Power available as fraction of sea level maximum: Maximum Continuous Cruise	Economy Cruise
0 to 17K	1.0	0.83
20K	0.889	0.708
25K	0.694	0.572
30K	0.514	0.425
35K	0.333	0.275

Example: HIPS airplane wing, pusher engine with laminar wing and fuselage.
Cruise power = 405 hp.
BHP_{TO} = 1216 hp.
Engine weight = 868 lb.

Fuel Consumption

Altitude (feet)	Specific fuel Consumption lb/hp/hr: Maximum Continuous	Economy Cruise
0 to 17K	0.313	0.290
20K	0.317	0.293
25K	0.323	0.293
30K	0.330	0.305
35K	0.336	0.311

4.4 Very Advanced Rotary Engine

The very advanced rotary is a turbocharged, water-cooled, high speed engine employing direct injection stratified charge. It is a scaled version of the RC2-32 engine design studied by Curtiss Wright (Reference 17).

Retracting apex seals are used to reduce friction at the cruise rpm of 5875 (equivalent). A simple centrifugal counterweight system is suggested to retract the seals at high rpm.

Stratified charge is achieved without a separate precombustion chamber by the use of two injectors per rotor, one rich and one lean. The use of stratified charge allows the engine to burn diesel, jet fuel, gasoline, or alcohol, for example, without injector modifications.

An advanced aluminum casting alloy, AMS 4229, is used for the rotor. This alloy has good strength-to-weight properties at the 400°F cruise rotor temperature. It is currently available from 15 foundries. A plasma-sprayed zirconium oxide coating is proposed for the rotor hot surface to reduce heat rejection into the oil by one-third and improve hydrocarbon emissions and engine efficiency. No other advanced materials are used; thus, the good specific weight of this engine does not depend on extensive use of high-temperature materials.

Cooling drag for the very advanced rotary is assumed to be negligible (Reference 15). In the past, water-cooled engine installations have been designed to provide a small amount of thrust due to heat addition to the air by the radiator.

Reference 15 reports test results for a nonturbocharged, low rpm, stratified charge engine which achieved bsfc's of 0.43 lb/bhp/hr (the RC1-350) at 1200 rpm. Advanced turbocharging is expected to allow a further reduction in bsfc, to 0.355 lb/bhp/hr. The stratified charge rotary is similar to the diesel in its ability to run well at very lean mixture ratios. Turbocharging improves efficiency by increasing engine output for the same friction loss and by permitting operation at optimum air/fuel ratios. Figure 4.5, from Reference 15, shows the qualitative effect of turbocharging on the fuel/air ratio and bsfc.

The test engine of Reference 15 had a relatively low specific power output; turbocharging might increase the specific power, but an increase in rpm is the major method used to provide high specific power output. The rotary engine is better suited to high rpm operation than a reciprocating engine, since it lacks valve components and large reciprocating masses. The expected specific weight of 0.90 lb/bhp for a 640 hp engine is achieved at an equivalent rpm of 5875 for cruise. Gearing is necessary to reduce the propeller rpm to 2000 at cruise. At this rpm, retracting apex seals are necessary to reduce friction to acceptable levels. The pressure loss due to the seal gap is small at high rpm.

Table 4.5 summarizes the characteristics of the very advanced rotary engine design. The 10 hp pressurization and cabin cooling requirement at cruise is added in the same manner as for the GATE engine. (See Section 4.1.)

Table 4.5 Very Advanced Rotary Engine Summary

Design Features

- Stratified charge using dual injectors
- Multifuel capability
- Very advanced turbocharging
- Liquid cooled--zero cooling drag
- Retracting apex seals
- Zirconium oxide insulated rotor face

Weight and Power

Weight: $W = .53\ (BHP_{TO} + \frac{10}{.55}) + 223.4$ (lb)

Power:

Altitude (feet)	Power available as fraction of sea level maximum	
	Maximum Continuous	Continuous Cruise
0 to 21K	1.0	0.781
25K	0.859	0.781
30K	0.709	0.65
35K	0.594	0.55

Example: HIPS airplane wing, pusher engine, laminar wing and fuselage.
Cruise power = 352 hp.
BHP_{TO} = 640 hp.
Engine weight = 572 lb.

Fuel Consumption

Altitude (feet)	Specific Fuel Consumption lb/bhp/hr	
	Maximum Continuous	Cruise
0 to 25K	0.372	0.355
30K	0.370	0.354
35K	0.378	0.357

4.5 Results of Propulsion System Analysis

Parametric trade studies were carried out using different values of wing loading and aspect ratio for each propulsion system. All configurations were assumed to employ a pusher propeller, laminar flow wing, and have some laminar flow on the fuselage. A conventional wing and tail planform was used along with an aluminum primary structure. All configurations were sized to meet the baseline mission performance specification.

Figures 4.6 - 4.9 show the takeoff gross weight, cruise specific range, and total fuel used for the baseline mission as a function of wing loading, for aspect ratios of 10 and 12, for each propulsion system. Several significant results are apparent. For the cruise speed and altitude chosen, the optimum wing loading in terms of fuel consumption is between 45 and 50 psf, regardless of engine type. It appears that aspect ratios higher than 12 would result in even better fuel performance than shown, but it is believed that 12 represents a practical upper limit because of internal fuel volume, structural elasticity, and internal space for control system and landing gear components. Note also that the curves are very flat at these optimum wing loadings, thus one would tend to choose a wing loading that is on the low side of the optimum value so that takeoff and landing speeds are as low as possible, consistent with efficient cruise performance.

Another observation is of interest regarding gross weight. In every case but one, the takeoff gross weight is lowered with an increase in aspect ratio from 10 to 12, even though wing weight will increase

as aspect ratio goes up. However, this structural weight increase is more than offset by the decrease in fuel weight and engine weight resulting from the improvement in aerodynamic efficiency. The exception is the GATE configuration, for which the higher aspect ratio produces a very slightly higher gross weight. This results from the fact that the GATE engine is very light weight, thus a reduction in engine weight due to lower drag is not sufficient to overcome the increase in wing weight.

Table 4.6 presents a comparison of the HIPS airplane, sized for the 1300 nm baseline mission, with four different advanced technology engines. Optimum values of wing loading and aspect ratio of 12 are used for the comparison.

The heaviest airplane is diesel powered; the lightest is the GATE, a result that corresponds directly with engine weight. On the other hand, the most fuel efficient airplane is rotary powered, a result of low engine weight, excellent specific fuel consumption, and negligible cooling drag. The gross weight of the rotary powered HIPS is only 17 lb heavier than the GATE powered HIPS. The GATE engine, with the highest sfc of all, uses the most fuel of any of the four configurations.

The diesel engine has the best specific fuel consumption, but this is offset by the relatively high specific weight and the high lapse rate of the diesel, which results in a sea level power rating about twice as large as the rotary and SIR.

As might be expected, the maximum and cruise L/D values are very nearly the same for all four configurations.

Considering fuel efficiency, gross weight, engine volume, engine cooling, and multifuel capability, the rotary powered HIPS appears

to be the most attractive configuration in this study. It is of interest at this point to note that the rotary powered HIPS configuration in Table 4.6 represents a 51.5% reduction in fuel used and a 15% reduction in gross weight compared to the original baseline HIPS configuration, with no change in mission performance.

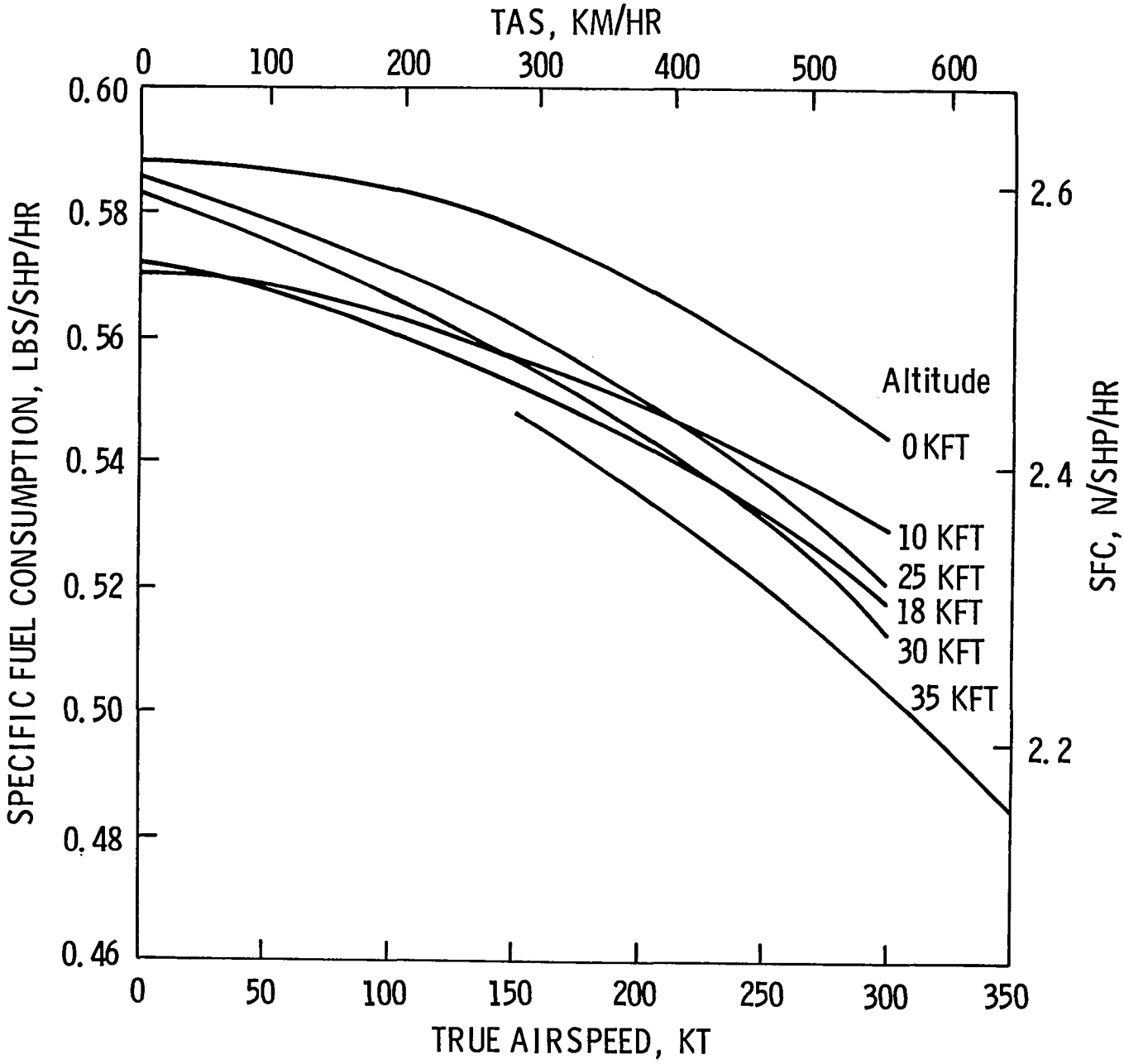

Figure 4.1 GATE Engine Specific Fuel Consumption

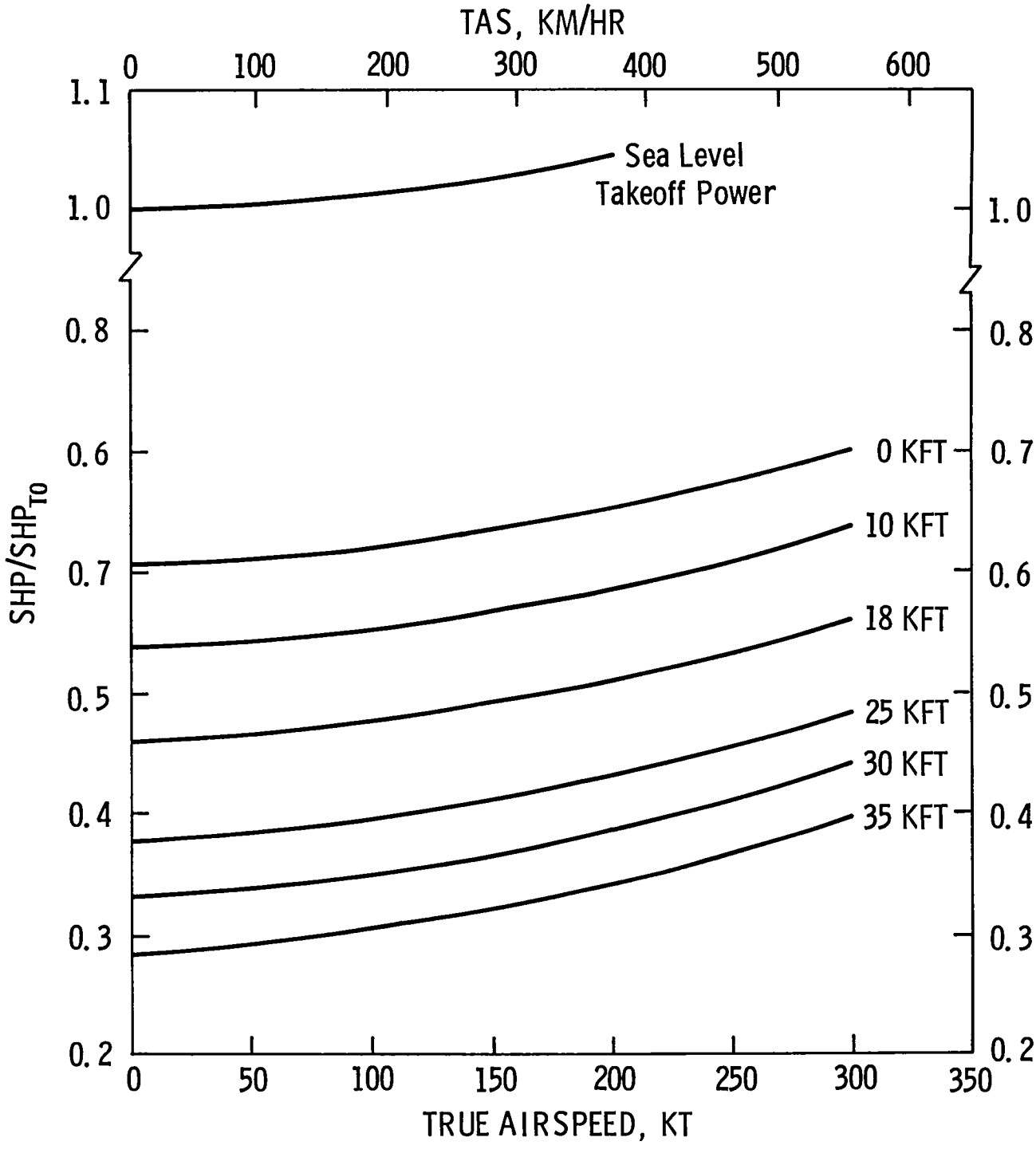

Figure 4.2 GATE Brake Horsepower Output

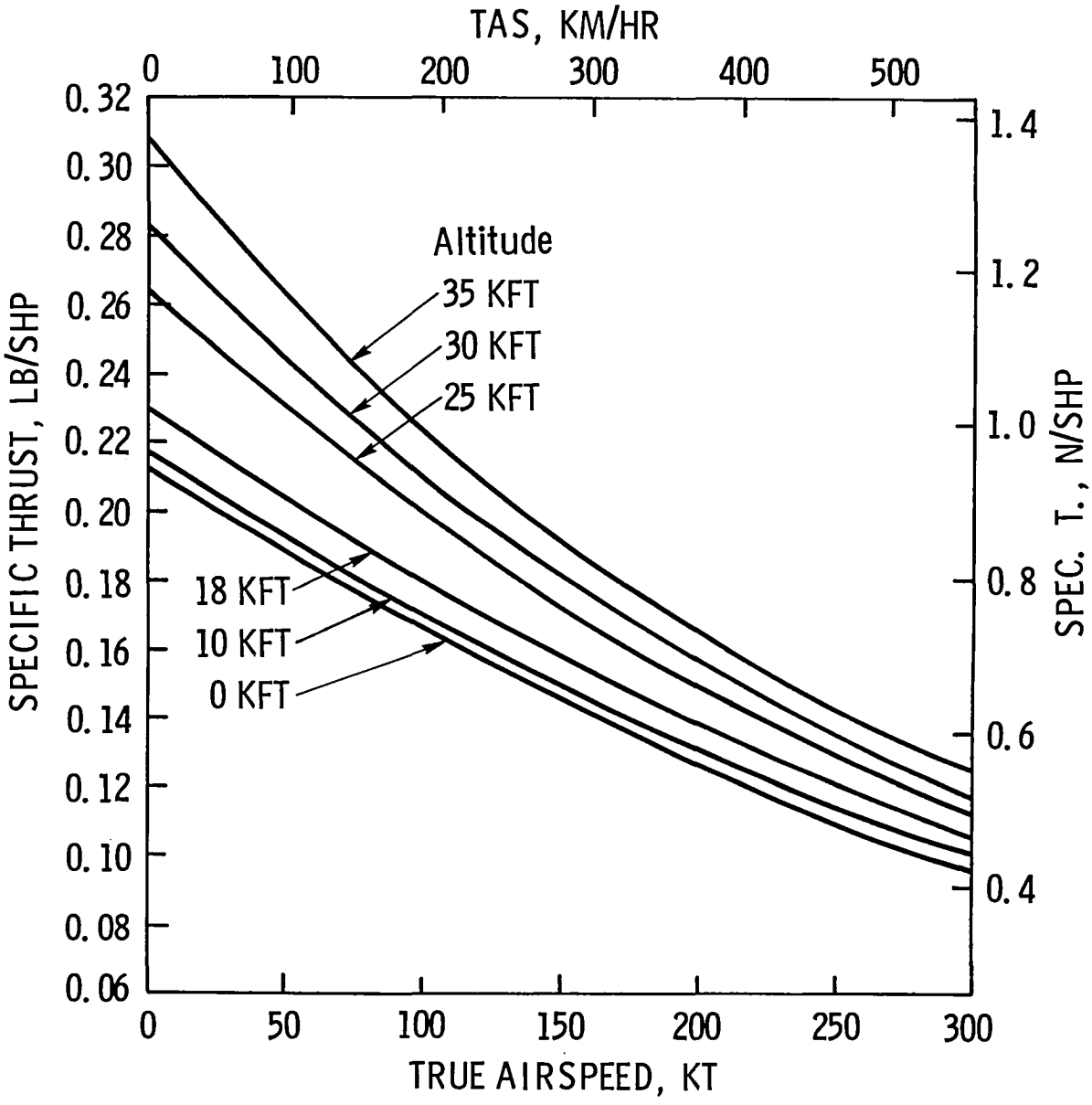

Figure 4.3 GATE Jet Thrust Output

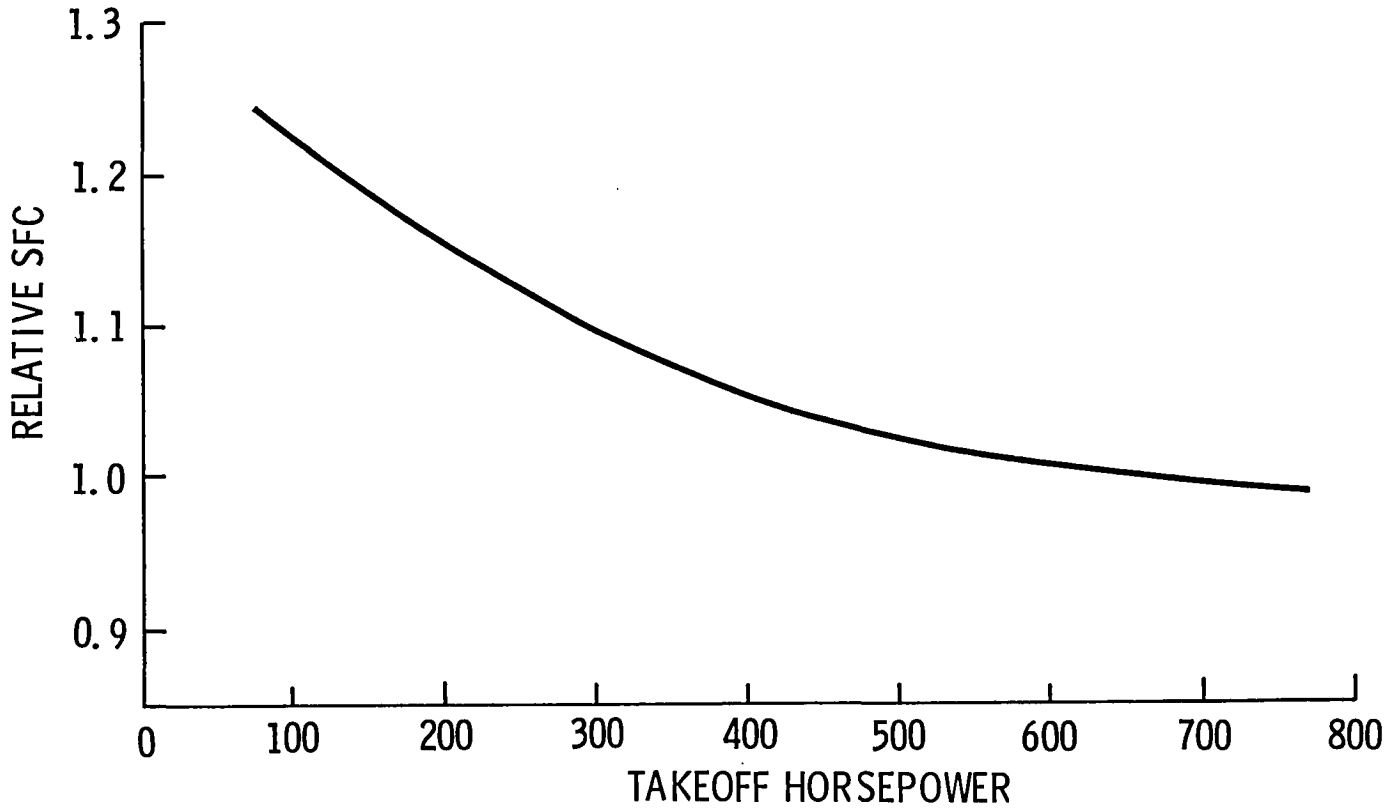

Figure 4.4 Effect of Engine Size on Specific Fuel Consumption of the GATE Engine

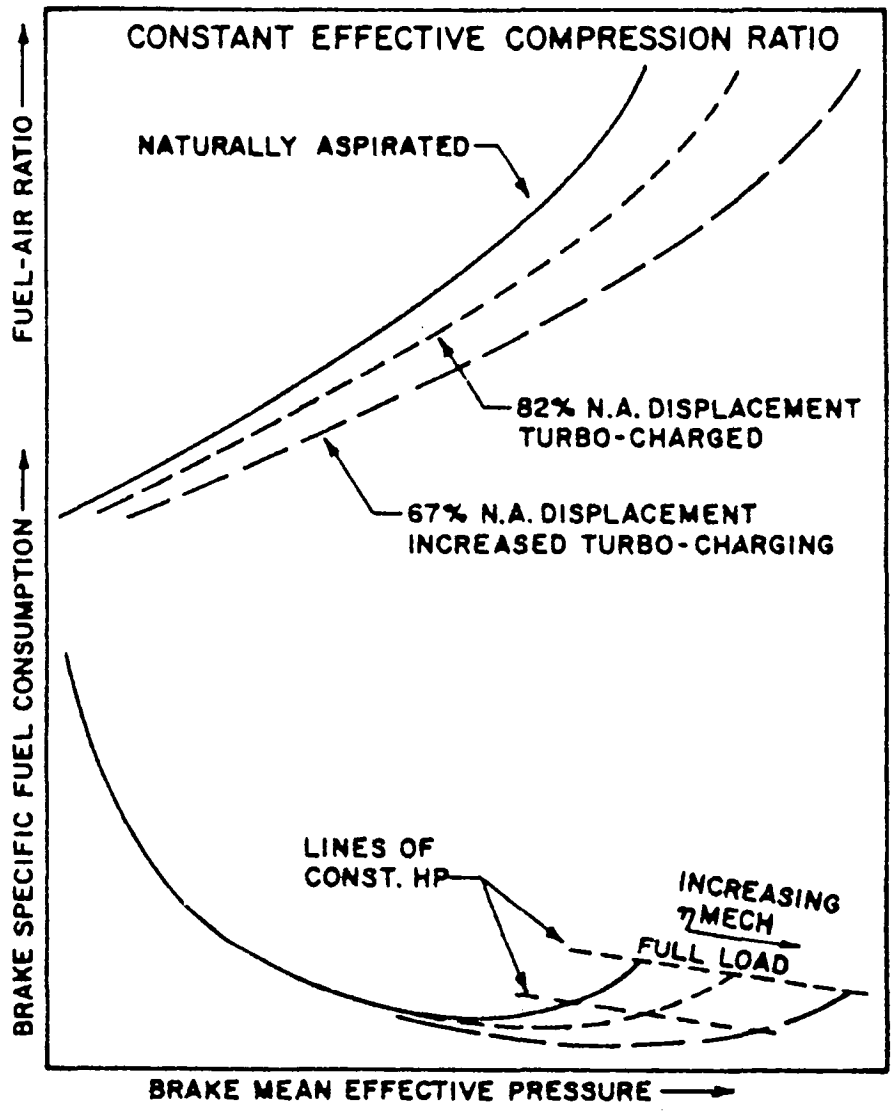

Figure 4.5 Effect of Decreasing Stratified Charge Rotary Engine Displacement, with Corresponding Increase in Degree of Turbo-Charging

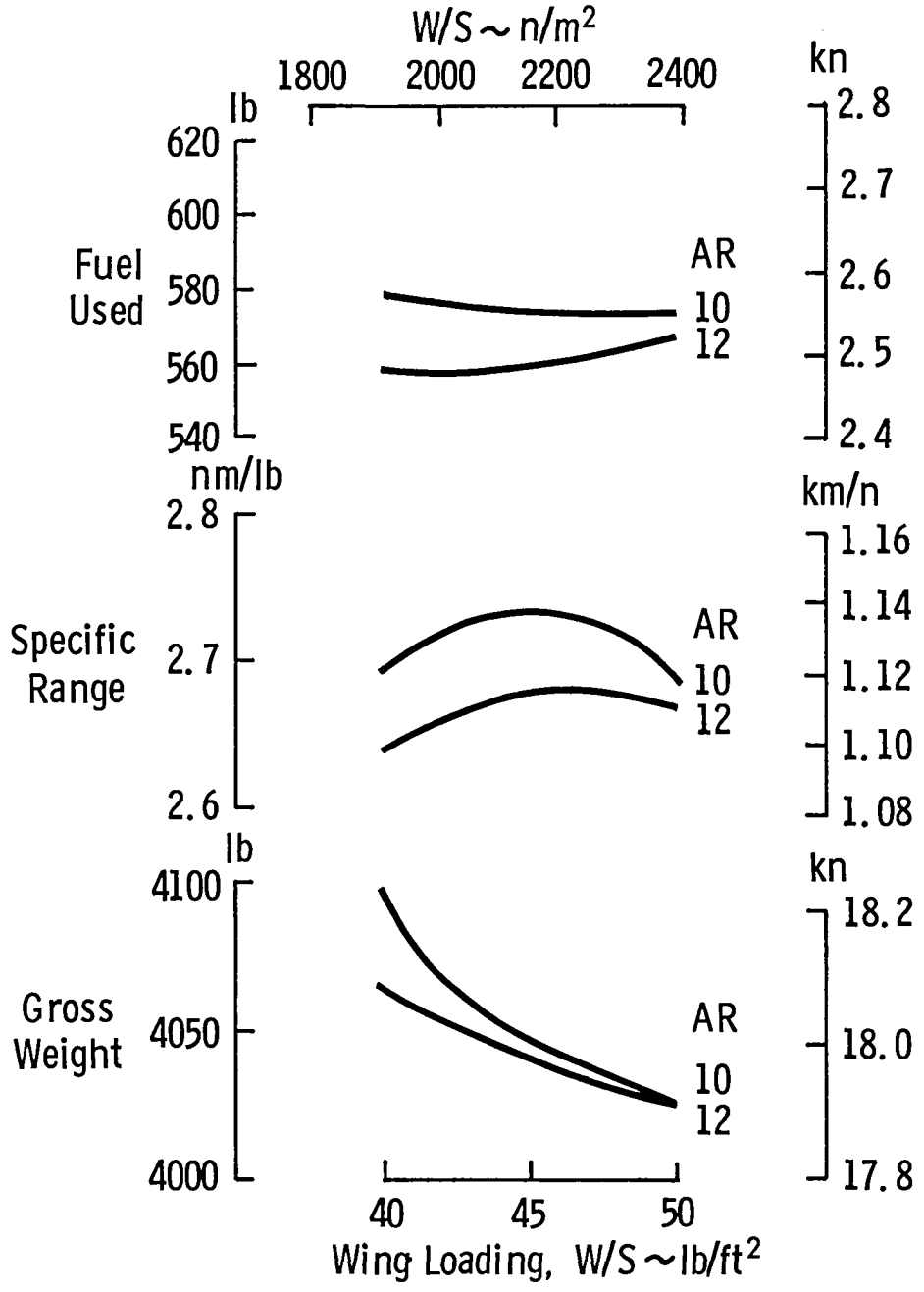

Figure 4.6 Fuel Requirements and Gross Weight Characteristics of an Advanced Single-Engine Airplane with a GATE Engine. Baseline Mission

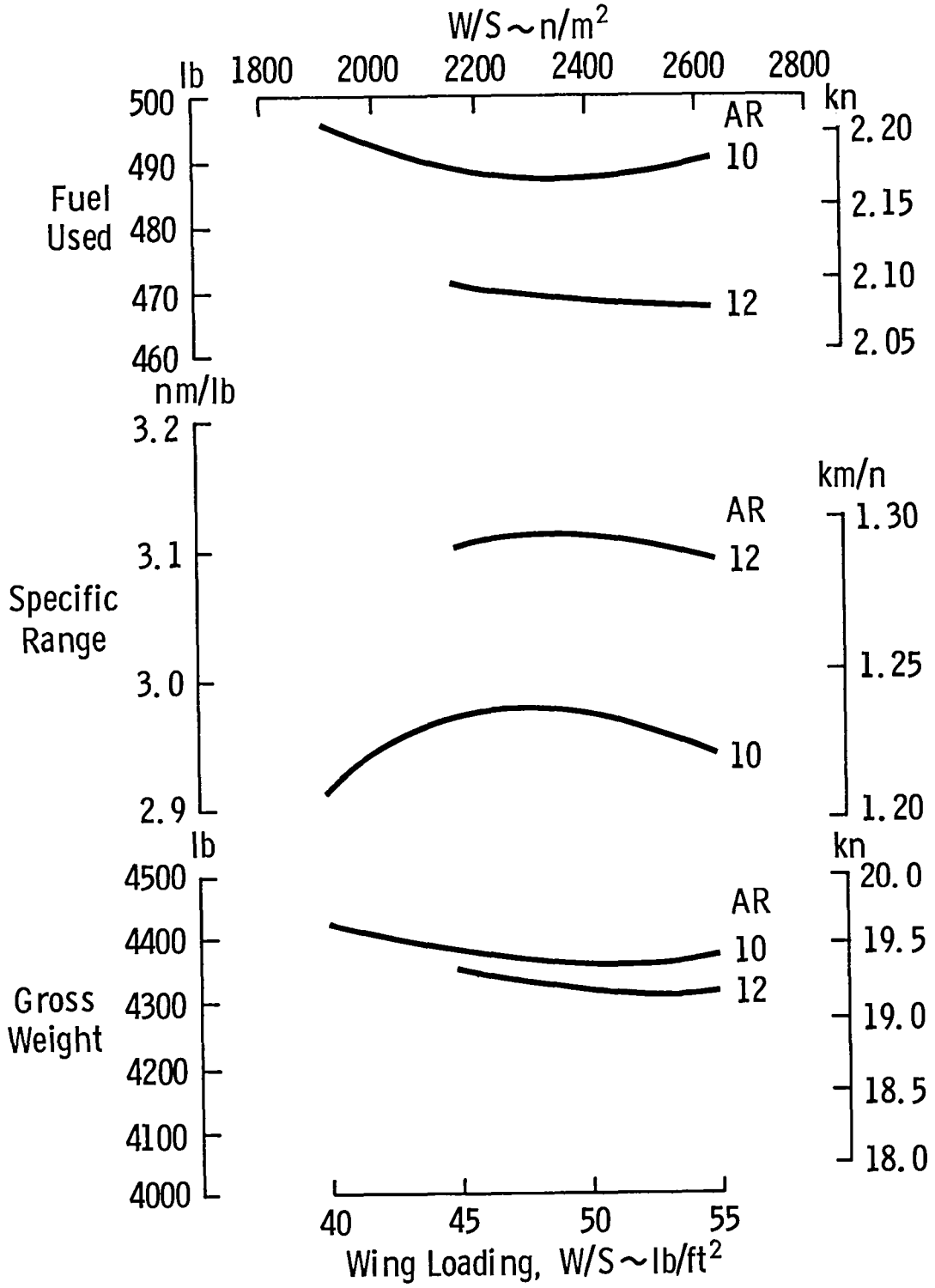

Figure 4.7 Fuel Requirements and Gross Weight Characteristics of an Advanced Single-Engine Airplane with a SIR Engine. Baseline Mission

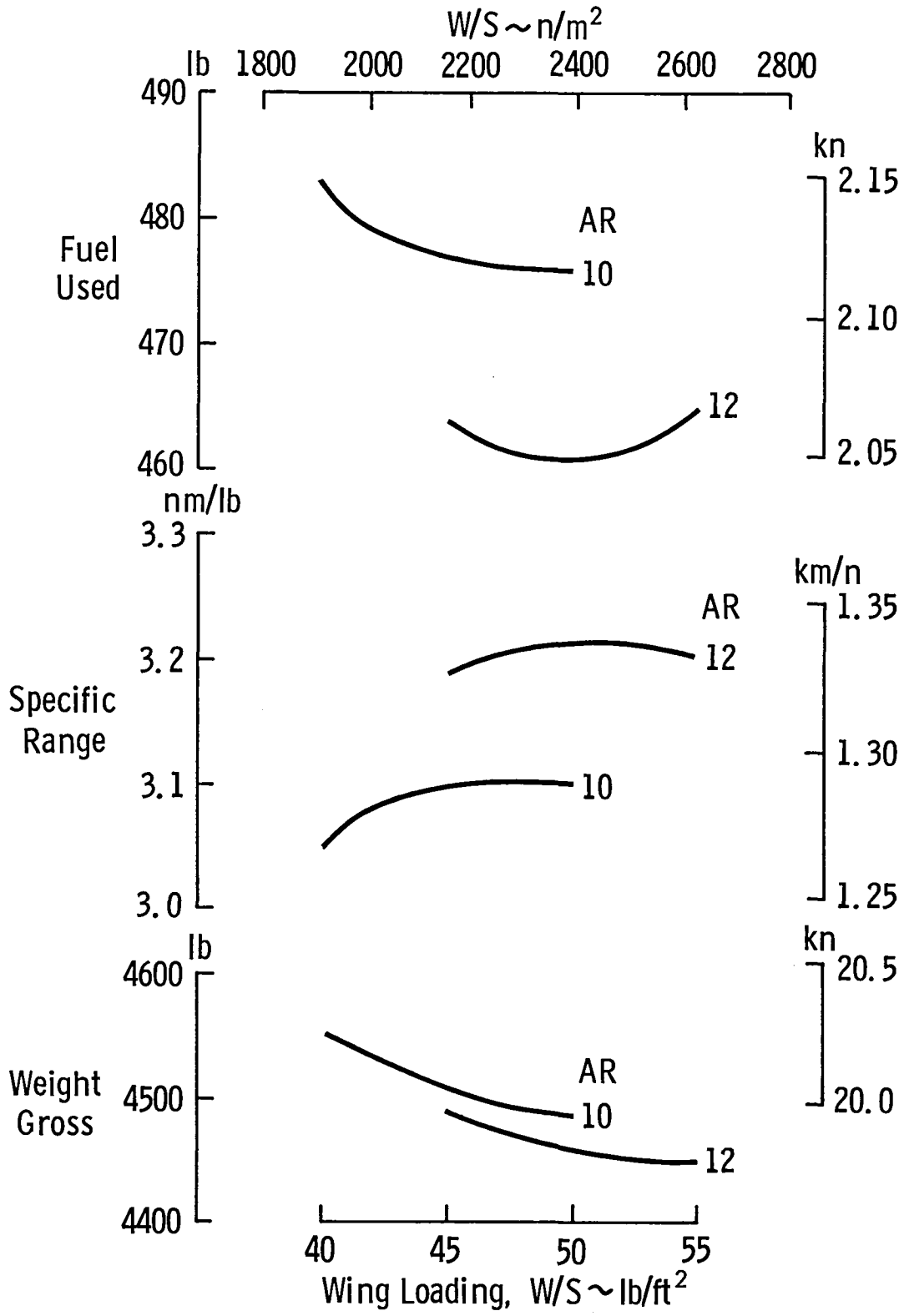

Figure 4.8 Fuel Requirements and Gross Weight Characteristics of an Advanced Single-Engine Airplane with a Diesel Engine. Baseline Mission

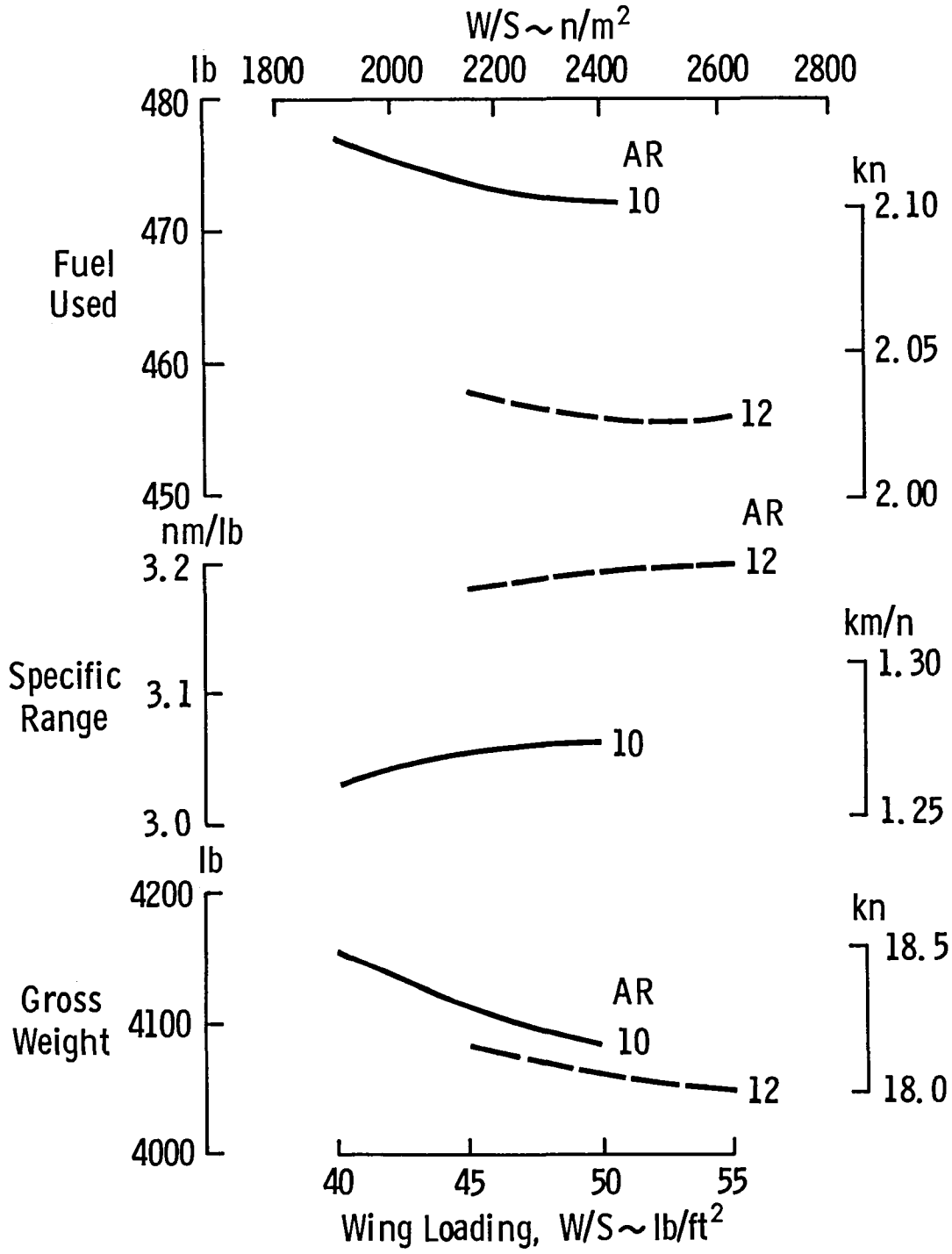

Figure 4.9 **Fuel Requirements and Gross Weight Characteristics of an Advanced Single-Engine Airplane with a Rotary Engine. Baseline Mission**

Table 4.6 Comparison of HIPS Airplane With Four Different Advanced Technology Engines

CONFIGURATION DATA	GATE	SIR	DIESEL	ROTARY
Gross Weight, lb	4045	4340	4458	4062
Wing Area, ft	89.9	86.8	89.2	81.2
Wing Loading, lb/ft^2	45.0	50.0	50.0	50.0
Aspect Ratio	12	12	12	12
Empty Weight, lb	2285	2673	2798	2406
Sea Level Max. Power, hp	806	573	1170	615
PERFORMANCE				
Average Cruise Specific Range, nm/lb	2.37	3.08	3.21	3.20
Total Fuel for Max. Payload Mission, lb (1300 nm Range)	560	468	461	456
Range (Max. Fuel), nm	1916	1864	1714	1564
(L/D) Max.	18.77	18.04	18.2	18.16
(L/D) Cruise (Average)	15.92	16.03	16.2	16.13

NOTE: All Configurations Incorporate Pusher Propeller, Laminar Flow Wing, Partial Laminar Flow Fuselage.

5. ELECTRIC PROPULSION SYSTEM ANALYSIS

5.1 System Description

The electric propulsion system analyzed for this report is a very advanced system based on data for the Mod II system of Reference 18. 1990 technology is assumed.

This system utilizes a low specific weight electric motor driven by the output of lithium fuel cells.

The d.c. electric motor is an advanced brushless design with a samarium-cobalt permanent magnet rotor. The efficiency of this motor is projected to be about 90% at full output. The specific weight is expected to be 0.25 lb/hp. For comparison, current high-output electric motors weigh about .75 lb/hp.

The lithium fuel cell concept is an evolutionary development from a current torpedo power system which uses lithium with hydrogen-peroxide oxidizer. For the advanced system, atmospheric oxygen is used to oxidize most of the lithium, with hydrogen peroxide available for high power demand such as takeoff. Atmospheric carbon dioxide reacts with the lithium to precipitate lithium carbonate for control of cell concentrations. The equations for the reaction of lithium with oxygen and carbon dioxide are:

$$LiOH + CO_2 \rightarrow Li_2CO_3 + H_2O$$

$$2Li + H_2O + \frac{1}{2} O_2 \rightarrow 2L_iOH.$$

The aircraft gains 4.29 lb in flight for every pound of lithium used, due to the necessity of retaining the lithium carbonate produced by the reaction. It is anticipated that the lithium carbonate can

be recycled. If not, the aircraft could lose weight in flight if dumping lithium carbonate is acceptable from an environmental standpoint. However, the cost would be significantly higher.

The energy content of lithium is 6280 watt·hr/lb, comparable to gasoline at 6044 watt·hr/lb (Ref. 3 and 4). About 65% of this energy is actually delivered to the load from the fuel cell. The electric motor is about 90% efficient, so the overall energy efficiency of the system is about 59%. For comparison, the energy efficiency of the aircraft diesel engine with a specific fuel consumption of 0.311 lb/hp/hr at cruise is about 42%. The current production TSIO-550 engine is about 29% efficient. The diesel engine therefore must reject about twice as much energy as heat for an equivalent useful power output. For a heat engine, much of this heat is rejected in the exhaust gases, and the rest must be carried away by cooling air. For the electrochemical fuel cell system, most of the excess heat is produced in the cell stacks, which will probably be located in the aircraft wings. Circulating the electrolyte through heat exchangers at the leading edge of the wing would be a natural way to remove this heat while providing protection from icing. A small amount of cooling airflow might be necessary for the electric motor. For this study, zero cooling drag was assumed.

The specific weight of the cell stacks and associated hardware is projected to be about .25 lb/hp. The weight of lithium required depends on the total energy required for the mission.

5.2 Performance Analysis

A HIPS aircraft using the advanced lithium fuel cell concept was sized to perform the same mission as the other HIPS designs, 1300 n.m. carrying a 1200 lb payload at a 300 knot cruise speed.

Some subroutine modifications were made to the General Aviation Synthesis Program (GASP) to accommodate the characteristics of the electric airplane. An engine subroutine was written to compute the power output with altitude for the fuel cells. A change was also needed in the routine which computes range.

The GASP range routine uses the Breguet range approximation to compute range during cruise. The usual Breguet equation was derived for airplanes that lose weight during flight. For the electric airplane, the Breguet approximation can be written as:

$$R = \frac{\eta}{sfc} \times \frac{L}{D} \log \frac{W1}{W0}$$

where: R = range

sfc = fuel consumption (specific weight gain in this case)

L/D = average lift-to-drag ratio

W1 = final weight

W0 = initial weight

η = propulsor efficiency.

Airplane designs were sized to fly at 35000 ft and 45000 ft cruise altitudes. Table 5.1 summarizes the characteristics of the resulting designs, compared with an airplane using an advanced rotary engine. It should be noted that the mission flown does not include a descent or landing phase. Because the electric airplane gains

Table 5.1: Characteristics of Electric and Very Advanced Rotary Engine Airplane Designs

	Electric			Rotary AR 12, W/S 50
	35000 ft.	45000 ft		35000 ft.
Cruise speed	300 knots	300 knots		300 knots
Engine T.O. h.p., sea level:	818	1154		615
Climb h.p.:	552	779		615
Weight breakdown:				
Electric motor:	205 lb.	289 lb.		
Cell stacks, plumbing:	307 lb.	721 lb.	engine install.	566 lb.
Propeller:	125 lb.	138 lb.		117 lb.
Aircraft structure:	1498 lb.	1634 lb.		1254 lb.
Controls, fixed eq.:	485 lb.	495 lb.		469 lb.
Payload:	1200 lb.	1200 lb.		1200 lb.
Lithium:	223 lb.	217 lb.	fuel	462 lb.
Takeoff weight:	4098 lb.	4759 lb.		4062 lb.
End-of-mission weight:	5100 lb.	5700 lb.		3600 lb.
Wing loading, start of mission:	40.2 psf	33.4 psf		50.0
end of mission:	50.0 psf	40.0 psf		44.3
Time to climb to cruise alt.:	0.35 hr.	0.34 hr.		0.34 hr.
Average cruise lift-to-drag:	16.97	19.91		16.13
$(L/D)_{max}$	19.37	20.73		18.16
Block time:	4.75 hr.	4.61 hr.		4.57 hr.

weight at cruise altitude, thus gaining potential energy, the electric airplane is penalized by not considering the descent phase.

The propulsion systems used for this study are "flat-rated"; that is, the fuel cells can put out more power at sea level than the electric motor is designed to accept. This reduces the electric motor weight.

The electric airplane configuration is the advanced baseline also used for the other four propulsion systems studied. It is conventional except for the use of a pusher engine arrangement. The wing aspect ratio is 12, and a NASA natural laminar flow airfoil is used. Credit is also taken for some laminar flow on the fuselage.

The 45000 ft cruise design consumes only 3% less lithium for this mission than the 35000 ft design. The greater weight of the larger cell stacks required for adequate output at 45000 ft offsets some of the advantage of flying higher. The 45000 ft airplane was designed with more power for takeoff and climb so that time-to-climb and block time would be nearly the same for the two designs. This increased the electric motor weight for the 45000 ft design.

An important variable in judging the value of the electric propulsion system is fuel cost. Projected cost for a moderate rate of use of lithium in the 1990 time frame is about $1.00 per pound. The best of the other advanced baseline propulsion system/airframe combinations, using the very advanced rotary engine, burns 456 lb of fuel for the 1300 n.m. mission. Total fuel cost at $2.00 per gallon (1990) is therefore about $150.00. For the fuel cell powered airplane, consuming 223 lb of lithium, estimated total fuel cost is $223 at $1 per

pound. For equal fuel costs, lithium would have to cost about $0.67/lb. A baseline airplane using a current technology airframe and a PT6 engine burns about 950 lb of fuel for the same mission. Thus, the fuel cell airplane with an advanced airframe is competitive with current technology aircraft in terms of fuel cost.

6. HIGH LIFT SYSTEM ANALYSIS

Possible performance increments were compared for three types of high-lift devices: leading-edge flaps, single-slotted Fowler flaps, and double-slotted Fowler flaps.

The increments in maximum lift coefficient computed by GASP were considered to be too high in all cases. Stall speeds were recomputed using $C_{L_{max}}$ values based on data from References [19] and [20].

The penalties for meeting the 61 kt single-engine stall speed requirement of the FAR's were found by comparing fuel used, total weight, and specific range for an airplane with the wing loading necessary for a 61 kt stall speed with values for an airplane with an optimum wing loading.

6.1 Trailing Edge Flaps

The GASP program computes maximum lift increments for trailing edge flaps as a function of flap type, wing geometry, and flap deflection. The clean wing maximum lift coefficient is calculated as a function of wing geometry, Mach number, and Reynold's number, based on the input value of the maximum lift coefficient for a reference wing with the desired airfoil section, and a reference geometry of aspect ratio 12, taper ratio 1, no quarter chord sweep, and a Reynold's number of 6×10^6. The GASP flap routine is based on methods presented in Reference 21.

The baseline flap system was a Fowler flap covering 75% of the wing span. Maximum lift coefficients computed by GASP for this system at various aspect ratios and a wing loading of 40 psf are listed in Table 6.1.

Table 6.1 Maximum Lift Coefficients Computed by GASP for the HIPS Airplane, 75% Span Single-Slotted Fowler Flap, W/S = 40 psf

AR	$C_{L_{max}}$ $\delta_f = 0$	$C_{L_{max}}$ $\delta_f = 40°$	$\Delta C_{L_{max}}$
6	1.27	2.64	1.37
8	1.32	2.81	1.49
10	1.35	2.89	1.54
12	1.36	2.90	1.54

The airfoil for the baseline airplane for the high lift system analysis was assumed to be a NACA 65_2-415 section, with no laminar flow. No data for single-slotted Fowler flaps were available for this particular airfoil, but Section 6.1.1.3-9 of Reference 19 lists a two-dimensional $C_{L_{max}}$ increment of 1.42 for a NACA 66_2-216 airfoil with a single slotted flap, and a two-dimensional $\Delta C_{L_{max}}$ of 1.75 for a NASA 23012 airfoil with a 30% chord, single-slotted Fowler flap. Reference 19, Section 6.1.4.3, suggests that about 70% of the two-dimensional $C_{L_{max}}$ increment should be available for a 75% span flap. On this basis a $C_{L_{max}}$ increment of about 1.2 to 1.3 should be available for a 75% span flap. Thus the three-dimensional $C_{L_{max}}$ values computed by the GASP flap routine and shown in Table 6.1 appear to be too high by approximately 0.2 to 0.3. For 75% span flaps, a $C_{L_{max}}$ value of 2.6 was used for an aspect ratio of 12 with the NACA airfoil.

For the advanced configurations, the use of the NLF-0516 airfoil increased the clean wing $C_{L_{max}}$ values by about 0.3. A $C_{L_{max}}$ of 2.8 was used for the NLF-0516 airfoil with 75% span single-slotted flaps.

The use of full-span, single-slotted and double-slotted Fowler flaps was investigated, with spoilers for roll control. $C_{L_{max}}$ values computed by GASP for full-span, single-slotted Fowler flaps are listed in Table 6.2.

Table 6.2 Maximum Lift Coefficients Computed by GASP for the HIPS Airplane, Full-Span Single-Slotted Fowler Flaps

AR	W/S	$C_{L_{max}}$ $\delta_f = 0$	$C_{L_{max}}$ $\delta_f = 40°$	$\Delta C_{L_{max}}$
10	40	1.67	3.49	1.82
10	50	1.68	3.48	1.80
12	45	1.71	3.54	1.83
12	50	1.70	3.53	1.83

Reference 19 suggests that about 92% of the two-dimensional $C_{L_{max}}$ increment should be available in three-dimensional flow for a full-span flap. Again, the computed $C_{L_{max}}$ values appear to be high by 0.2 or 0.3. Therefore, a $C_{L_{max}}$ value of 3.2 was used to compute stall speeds for the airplane with the NLF-0516 airfoil and full-span single-slotted flaps.

For double-slotted flaps covering 75% of the wing span, $C_{L_{max}}$ values computed by GASP were:

AR	W/S	$C_{L_{max}}$ clean	$C_{L_{max}}$ 40° flaps	$\Delta C_{L_{max}}$
12	50	1.71	3.74	2.03

Reference 19 lists a two-dimensional $C_{L_{max}}$ increment of 1.91 for a NACA 23012 airfoil with a 40% chord, double-slotted flap. This was the highest $\Delta C_{L_{max}}$ value reported in Reference 19. The three-dimensional increment would be about 1.34 for this case with a 75% span flap. Values predicted by GASP were approximately 0.7 higher than this. A $C_{L_{max}}$ value of 2.93 was used to compute stall speeds for this case. A $C_{L_{max}}$ value of 3.35 was used to compute stall speeds for double-slotted, full-span flaps on the NLF-0516 wing.

Stall speeds were calculated for various wing loadings and flap configurations using values for $C_{L_{max}}$ estimated from Reference 19 data, as noted above. Table 6.3 is a summary of stall speeds for various wing loadings, including the approximate wing loading for a 61 kt stall speed in the landing configuration.

The $C_{L_{max}}$ values estimated for Table 6.3 are comparable to those of two existing aircraft. The Mitsubishi MU-2N has a trimmed $C_{L_{max}}$ of 3.08, and the American Jet Hustler prototype demonstrated a trimmed $C_{L_{max}}$ of 3.2--both with full-span Fowler flaps (calculated from Reference 20 data). The wing loading limitations necessary to achieve a 61 kt stall speed cause some penalties in cruise efficiency with the flap systems considered above. Penalties in fuel used to meet the 61 kt requirement for the baseline and advanced rotary airplanes are listed in Table 6.3.

Takeoff and landing distances for all the flap systems and wing loadings studied are well under the 3000 ft limit.

Table 6.3 Stall Speeds and Wing Loading Limits for Various Flap Configurations

Aifoil and Flap Type		PT6 Engine, Baseline, NACA 65_2-415 Airfoil, 0.75 Span, Single-Slotted Flap, $C_{L_{max}} = 2.6$	Rotary Engine, NLF-0516 Airfoil Single-Slotted 0.75 Span Flap, $C_{L_{max}} = 2.8$	Rotary Engine, NLF-0516, Full Span, Single-Slotted Flap, $C_{L_{max}} = 3.2$	Rotary Engine, NLF-0516, 0.75 Span, Double-Slotted Flap, $C_{L_{max}} = 2.93$	Rotary Engine, NLF-0516, Full Span, Double-Slotted Flap, $C_{L_{max}} = 3.35$
AR	W/S lb/ft^2	Stall Speed kt	Stall Speed kt	Stall Speed kt	Stall Speed kt	Stall Speed kt
12	30	58.4				
12	35		50.8	56.8	59.4	55.5
12	40	67.4	65.0	60.8	63.5	59.4
12	45		68.9	64.4	67.3	63.0
12	50	75.4	72.6	67.9	71.0	66.4
12	55		76.2	71.2	74.5	69.6
Wing Loading Limit for 61 kt Stall		32.8 psf	35.3 psf	40.3 psf	36.9 psf	42.2 psf
Penalty for Meeting 61 kt Stall Requirement	Fuel Used	+14%	+6.9%	+2.4%	+6.4%	+1.5%
	Gross Weight	+8.4%	+6.0%	+1.5%	+4.6%	+1.0%
	Engine Size	+13%	+6.7%	+2.5%	+6.3%	+1.5%

6.2 Leading Edge Flaps

Leading edge flaps are employed primarily on relatively thin airfoils with small leading edge radii which exhibit leading edge stall, such as the high-speed airfoils used on transport aircraft. However, slots or slats have been used on thicker airfoils on some STOL aircraft. The $C_{L_{max}}$ increment obtained with leading edge devices is very dependent on the airfoil type, the design of the leading and trailing edge flaps, and, to some extent, the trailing edge flap deflection.

Leading edge devices might allow an increase of 0.3 to 0.5 in $C_{L_{max}}$, which would increase the wing loading limit for a 61 kt stall speed to 46-48.5 psf for full-span, double-slotted flaps and 40.7-43.2 psf for 0.75 span double-slotted flaps. However, with a retractable slat it is difficult to obtain a smooth contour of the wing skin when the slat is retracted. A step or gap could cause transition to turbulent flow near the nose of the airfoil.

With the possibility of reduced wing laminar flow and the increased cost and complexity, leading edge devices are not considered to be worthwhile for these designs. Even if complete laminar flow could be maintained, the gain in fuel efficiency using a leading edge device is only one or two percent when combined with a double-slotted flap system. The loss in fuel efficiency if laminar flow is not maintained could be as much as 14% (see Section 3.4).

7. EFFECT OF MISSION PARAMETERS

The baseline mission (Table 3.1) selected for this study is somewhat arbitrary. Nevertheless, it was defined with specific objectives in mind. The cruise speed of 300 knots is near the practical upper limit for propeller-driven airplanes currently in production and represents a 50% to 100% increase above the cruise speed of current high-performance, single-engine airplanes. The range of 1300 nm is comparable with that of most twin-engine piston and turboprop airplanes available today and is a significant improvement over virtually all current single-engine airplanes (see Figure 1.1).

It is desirable, however, to assess the sensitivity of the airplane performance parameters and configuration to changes in the mission speed, range, and payload. The following sections present data that resulted from such a study.

7.1 Effect of Cruise Speed

To determine the effect of cruise speed, the airplane was sized to the baseline mission except that cruise speeds were set at 200, 250, 300, and 350 knots. At each speed, variations were made in wing loading and aspect ratio to determine optimum fuel efficiency. This was done for each of the four propulsion systems described in Chapter 4. The results are presented in Figures 7.1 through 7.11. The GATE engine was analyzed at 350 knots for only one configuration--aspect ratio of 12 and wing loading of 50 lb/ft^2--because of convergence difficulties with that particular engine at the highest airspeed.

The effect of cruise speed is summarized in Figure 7.12, which shows the effect of cruise speed on total fuel, specific range during cruise, and takeoff gross weight with no change in the 35,000 ft cruise altitude. These data represent optimum values of wing loading at each speed with aspect ratio of 12.

It is clear that an increase in cruise speed exacts a penalty in fuel efficiency and gross weight. For example, a 50 percent increase in cruise speed, from 200 to 300 knots, results in a 20 to 30 percent increase in total fuel used for the 1300 nm mission, and a 16 to 23 percent reduction in cruise specific range. The corresponding increase in gross weight is less than 100 lb (about 2.5 percent).

7.2 Effect of Range

The airplane was sized for range performance varying from 900 to 1700 nm. All other baseline mission requirements were held constant. The results are presented in Figure 7.13 for each of the four propulsion systems, using an aspect ratio of 12 and optimum wing loading. A 31% (400 nm) change in range requirement from the nominal 1300 nm results in approximately a 29% change in total fuel and about a 5% change in takeoff gross weight. Specific range during cruise increases as range decreases by almost exactly the percent decrease in gross weight.

7.3 Effect of Payload

A study of the effect of payload on gross weight and fuel consumption was conducted by sizing airplanes with four different propulsion systems to the basic mission, except for payload which was varied over the range from 800 to 1600 lb. Results are presented in Figure 7.14 for airplanes with optimum wing loading and aspect ratio of 12.

Fuel required for the mission is almost a linear function of payload. A 1.0 lb change in payload results in approximately a 0.15 lb change in fuel required. Cruise specific range changes vary from 9% to 15% for a 50% change in payload, and gross weight increases about 1.67 to 2.0 lb per pound of payload, depending on engine type.

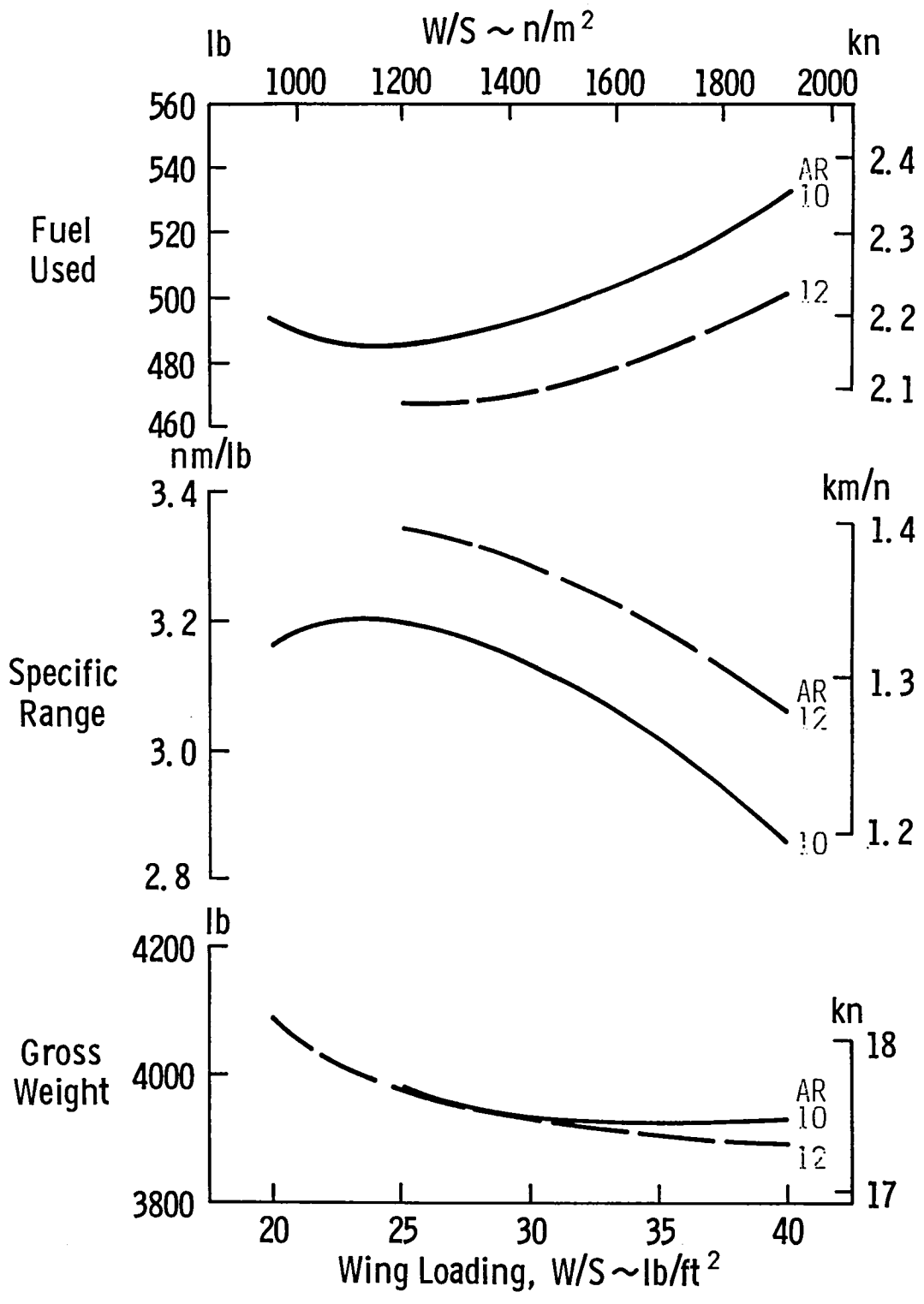

Figure 7.1 Effect of Wing Loading with 200 KTS Cruise Speed, GATE Engine.

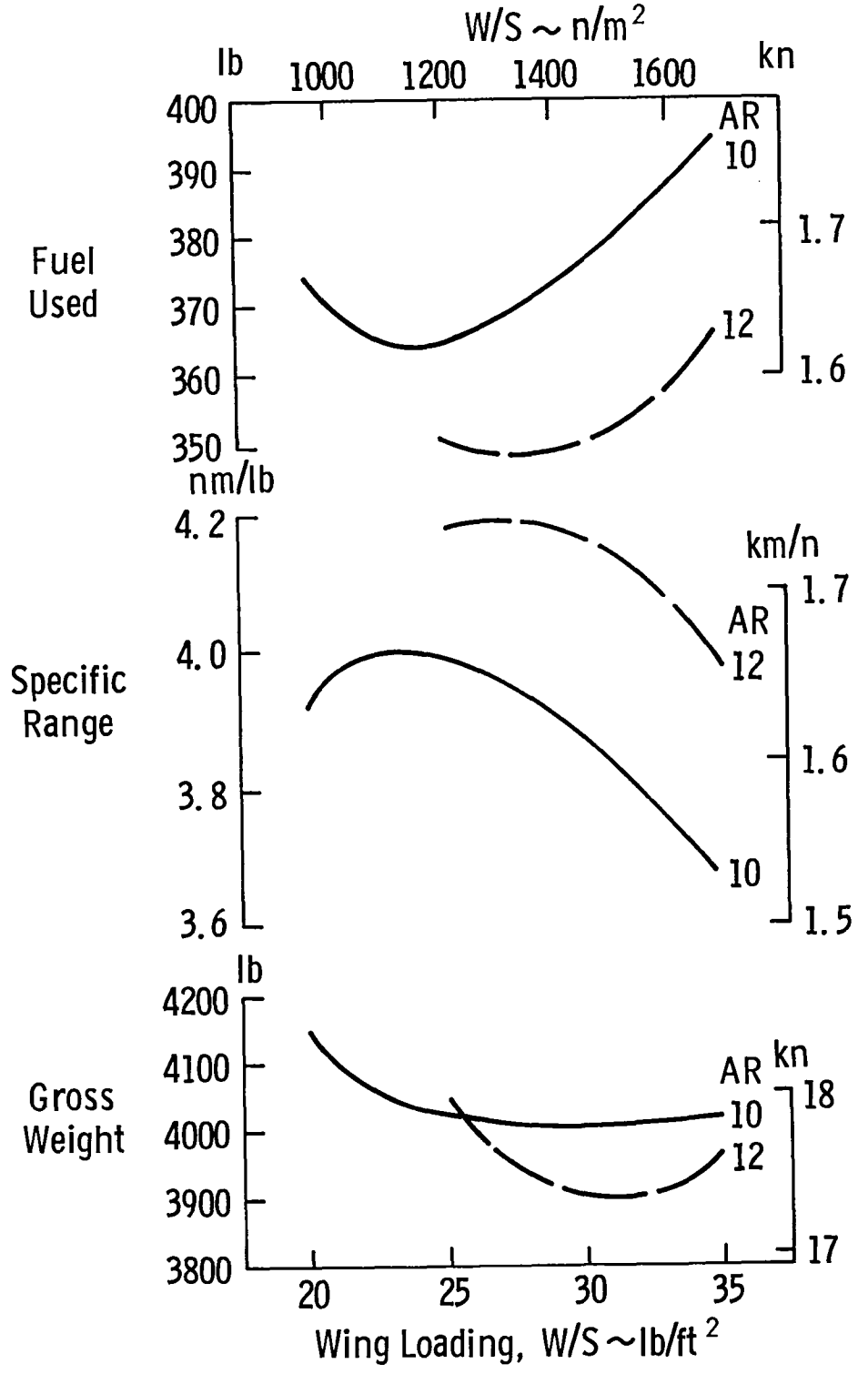

Figure 7.2 Effect of Wing Loading with 200 KT Cruise Speed, SIR Engine

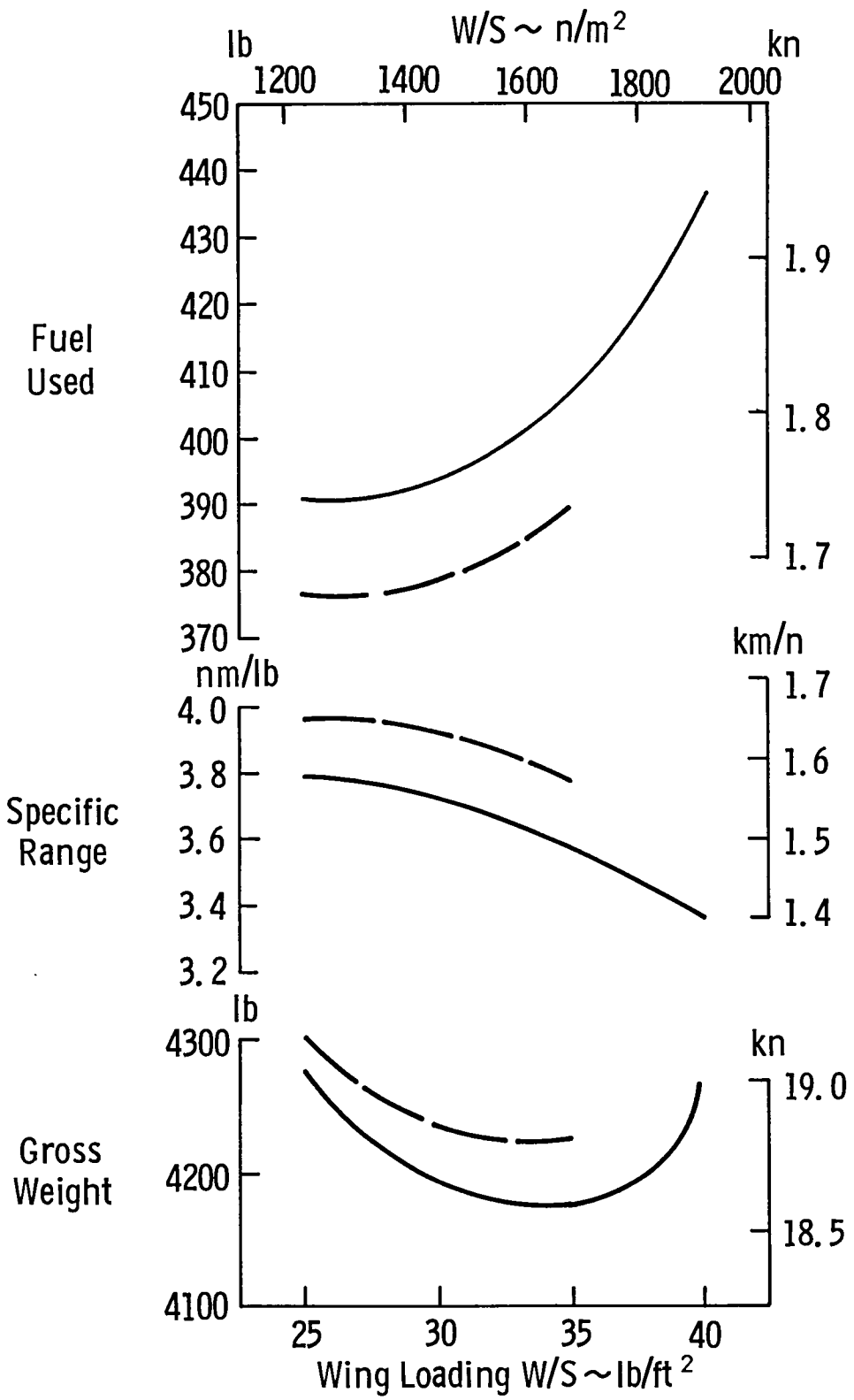

Figure 7.3 Effect of Wing Loading with 200 KT Cruise Speed, Diesel Engine

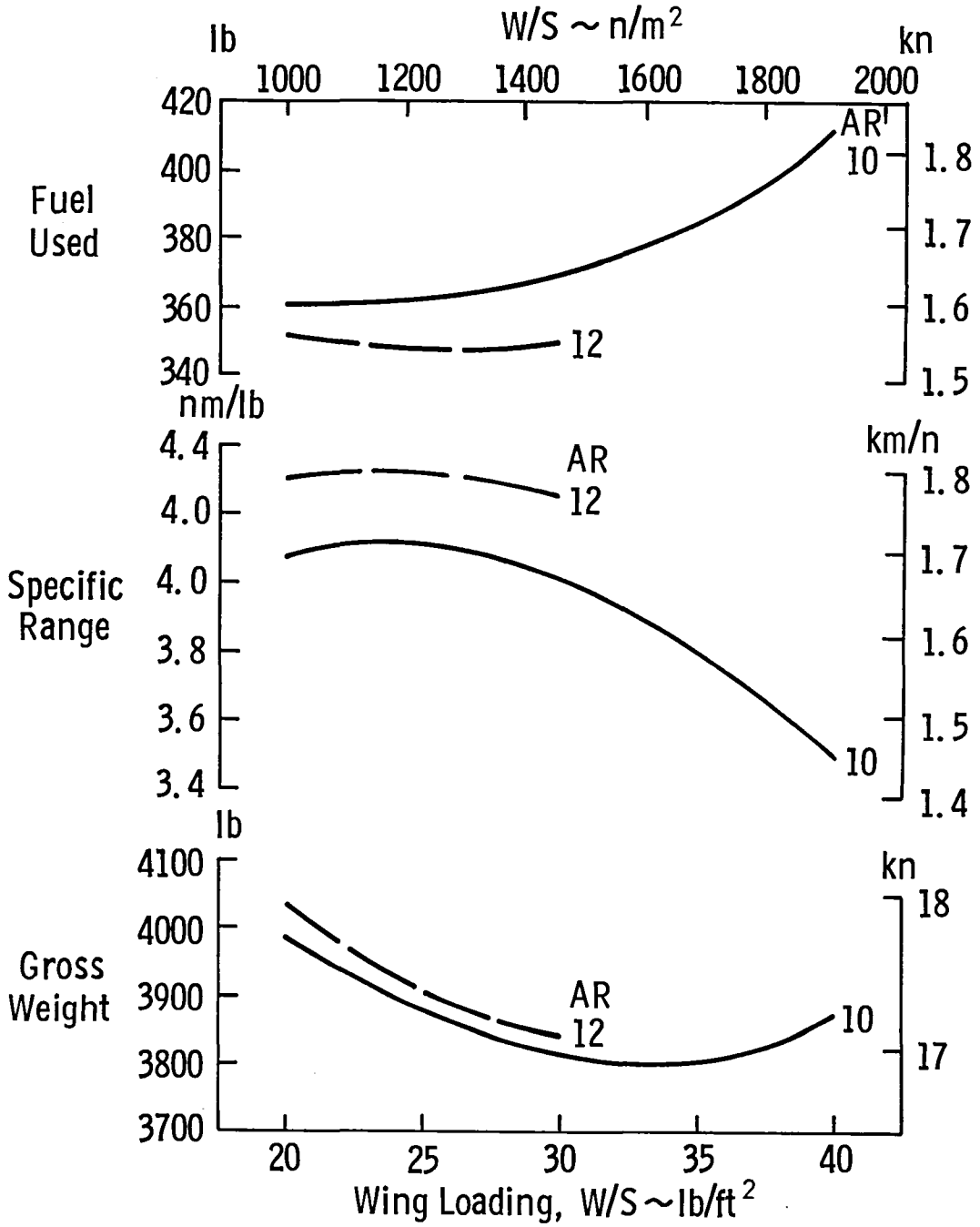

Figure 7.4 Effect of Wing Loading with 200 KT Cruise Speed, Rotary Engine

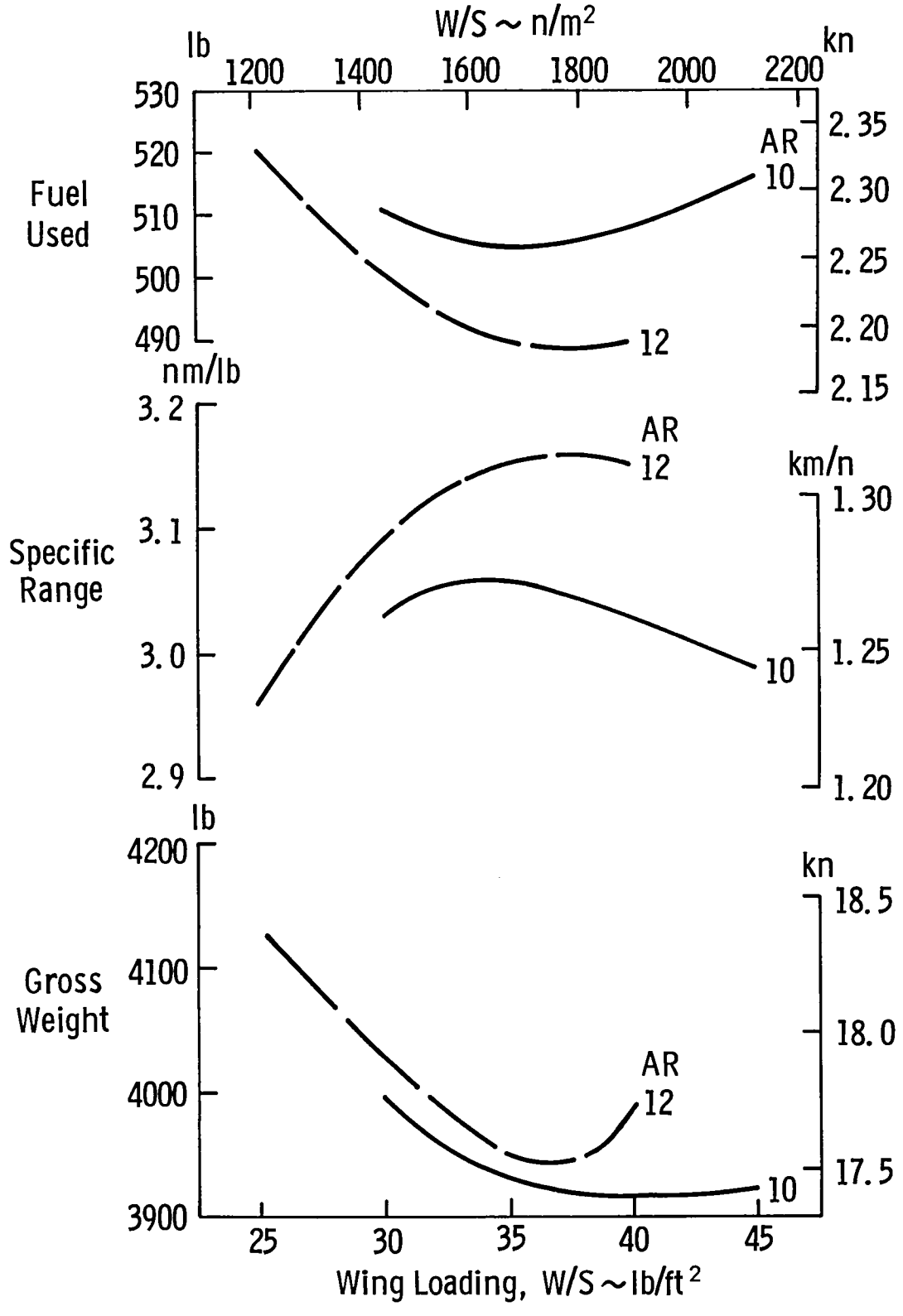

Figure 7.5 Effect of Wing Loading with 250 KT Cruise Speed, GATE Engine

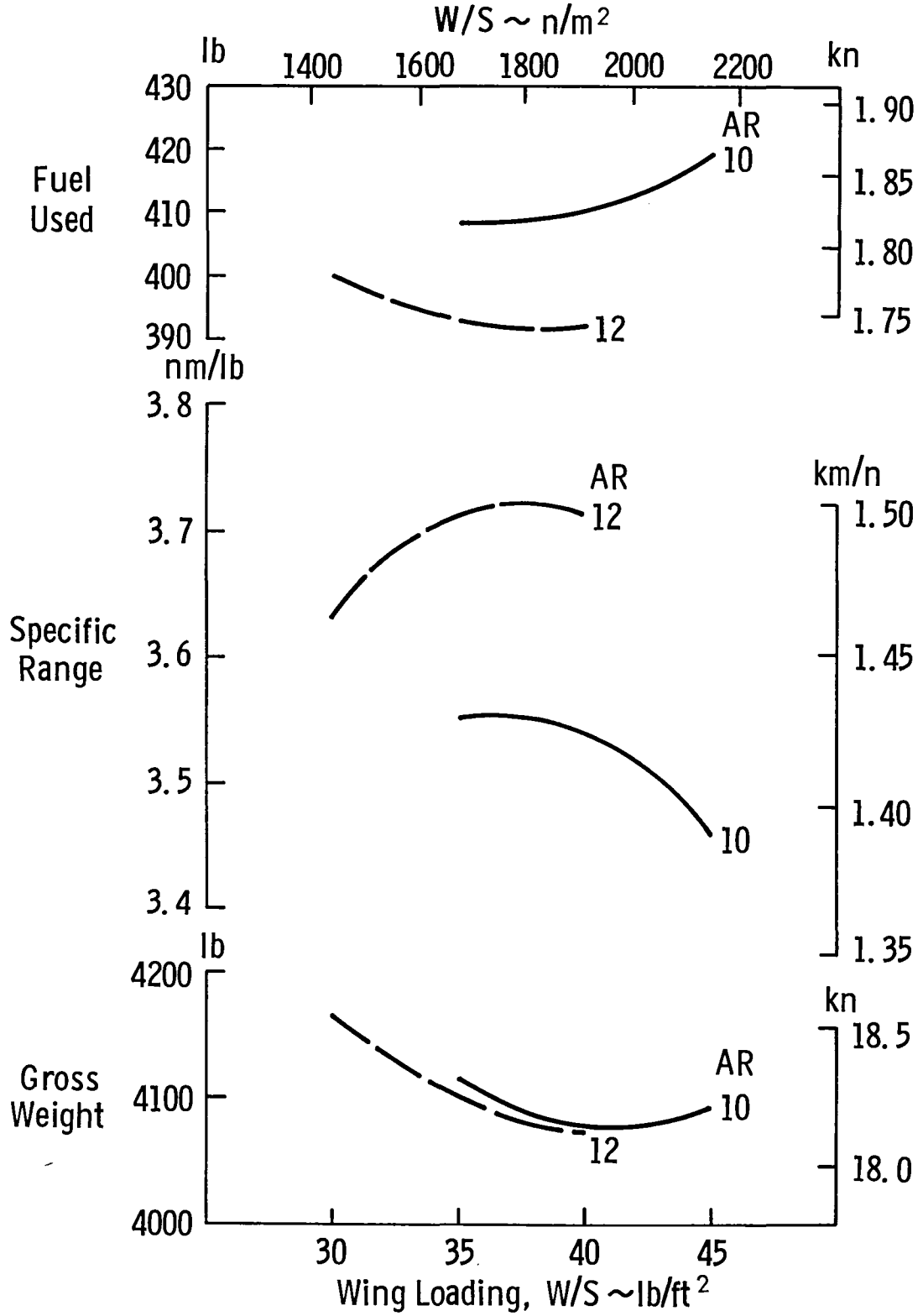

Figure 7.6 Effect of Wing Loading with 250 KT Cruise Speed, SIR Engine

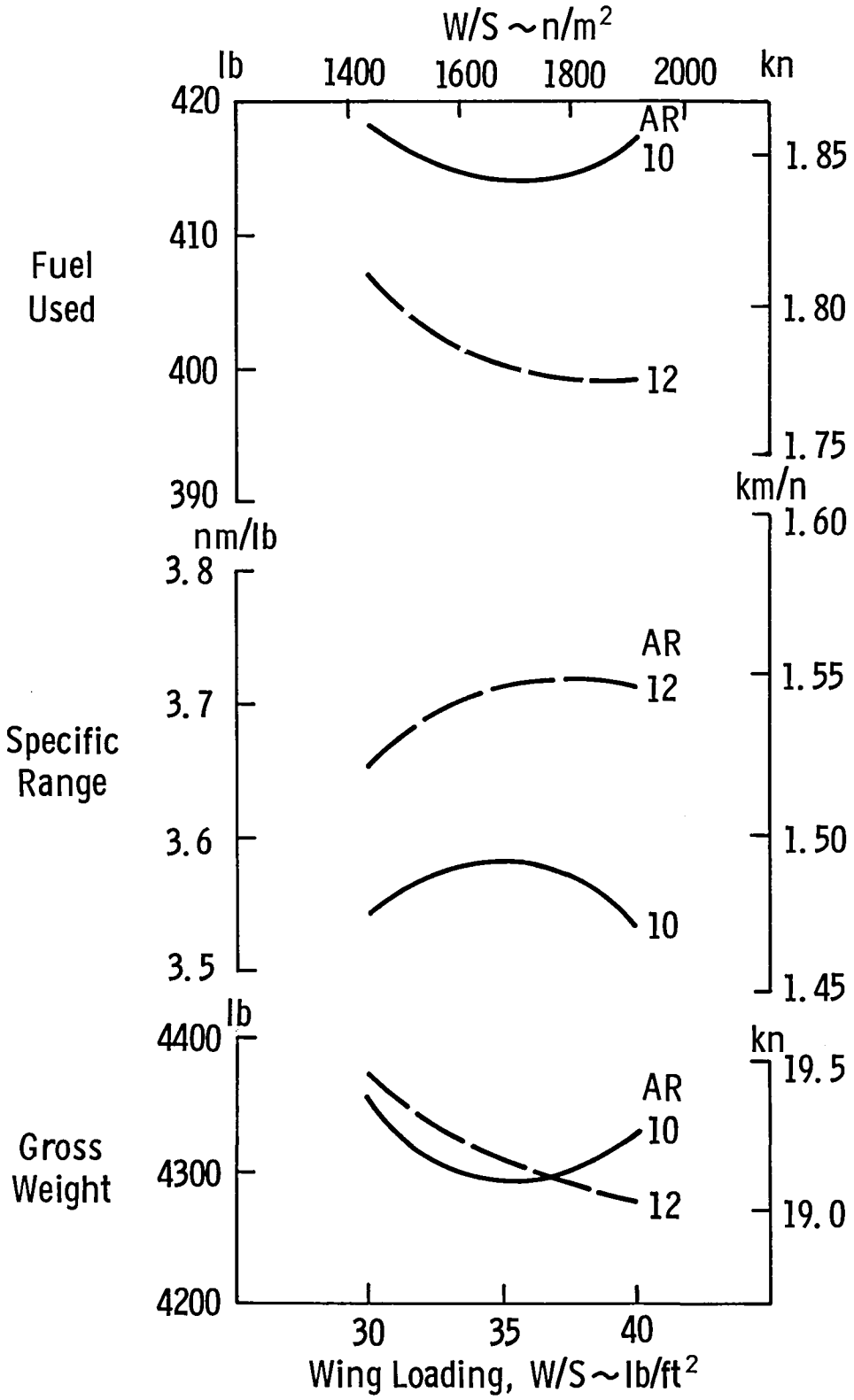

Figure 7.7 Effect of Wing Loading with 250 KT Cruise Speed, Diesel Engine

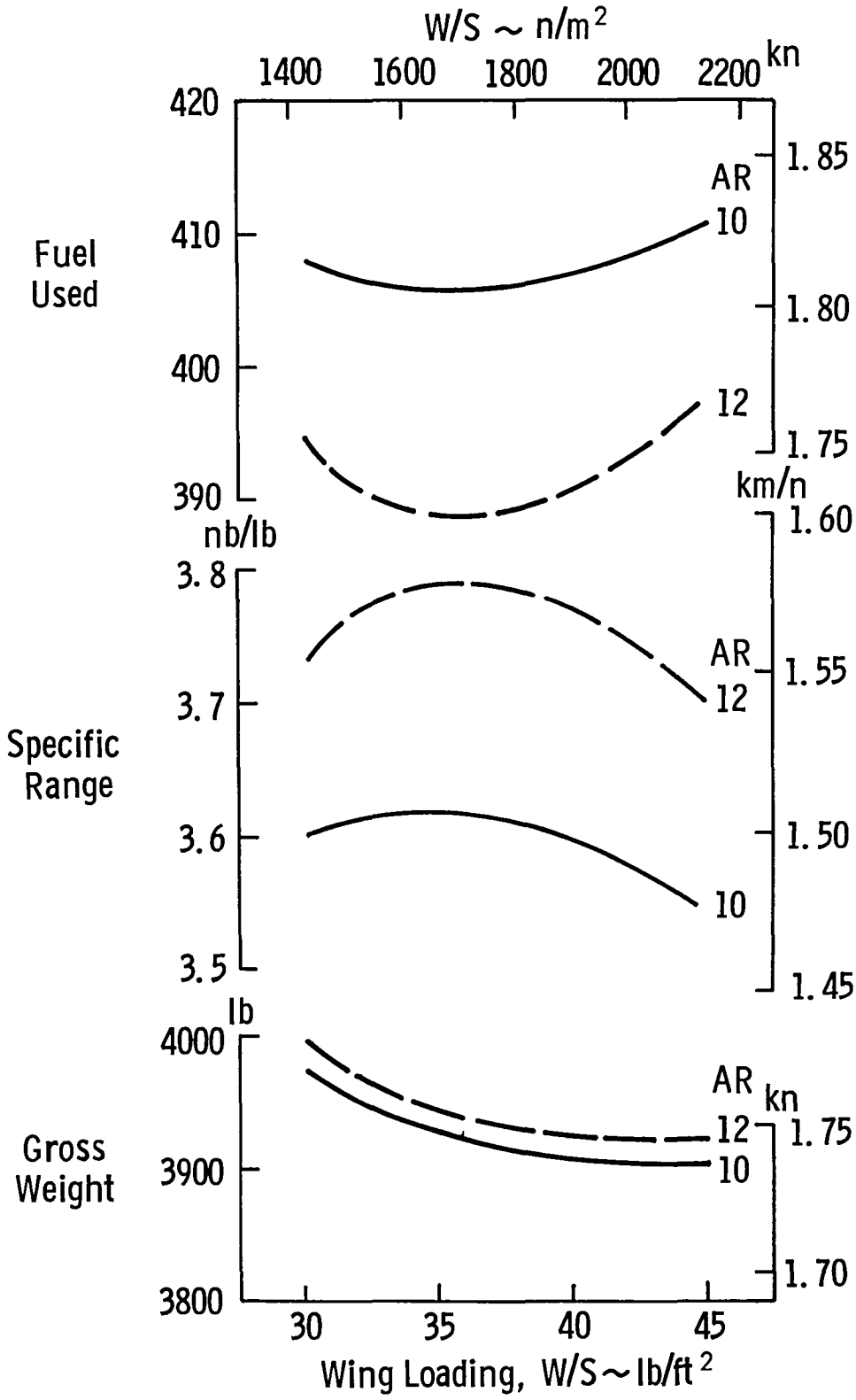

Figure 7.8 Effect of Wing Loading with 250 KT Cruise Speed, Rotary Engine

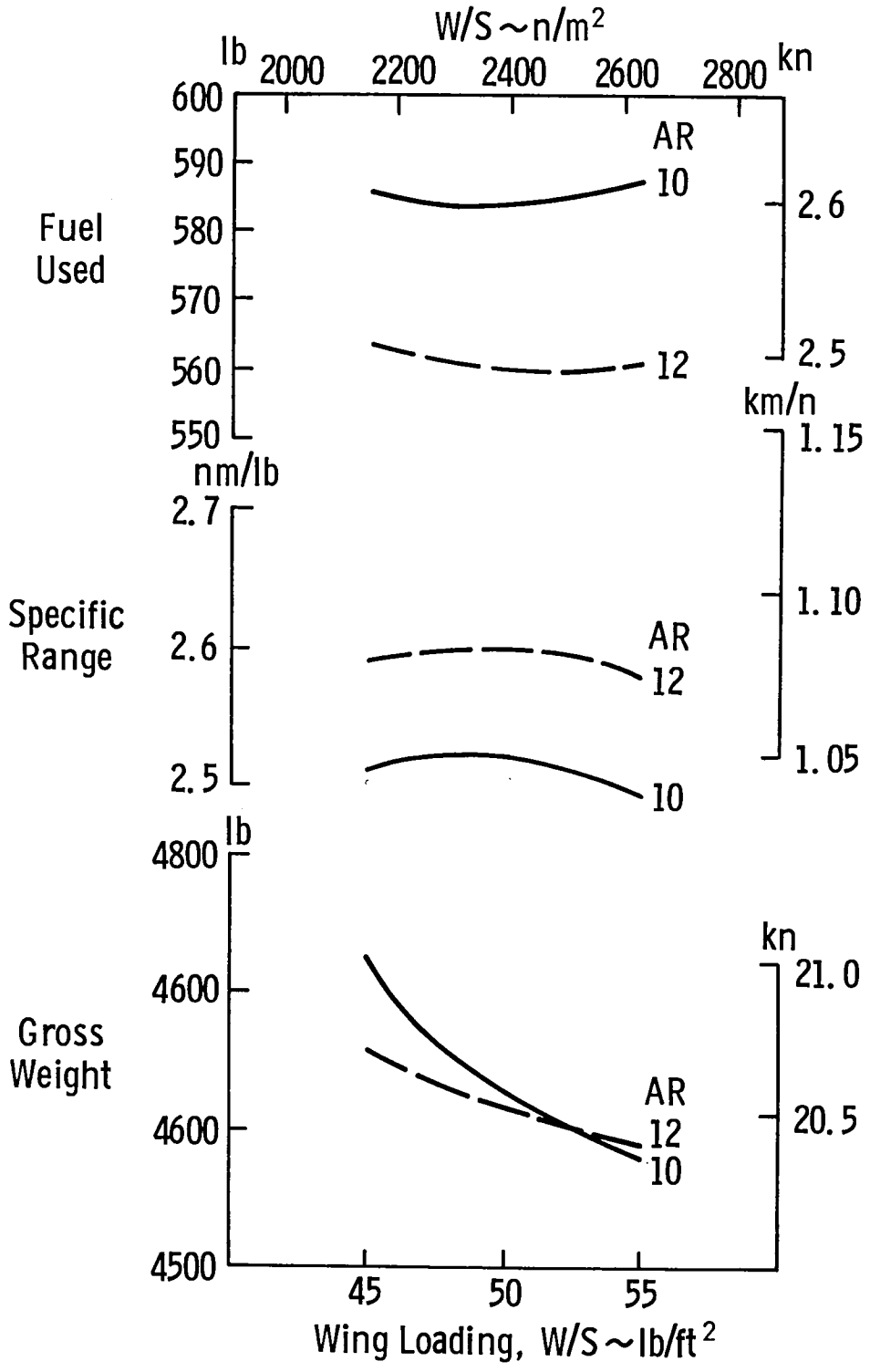

Figure 7.9 Effect of Wing Loading with 350 KT Cruise Speed, SIR Engine

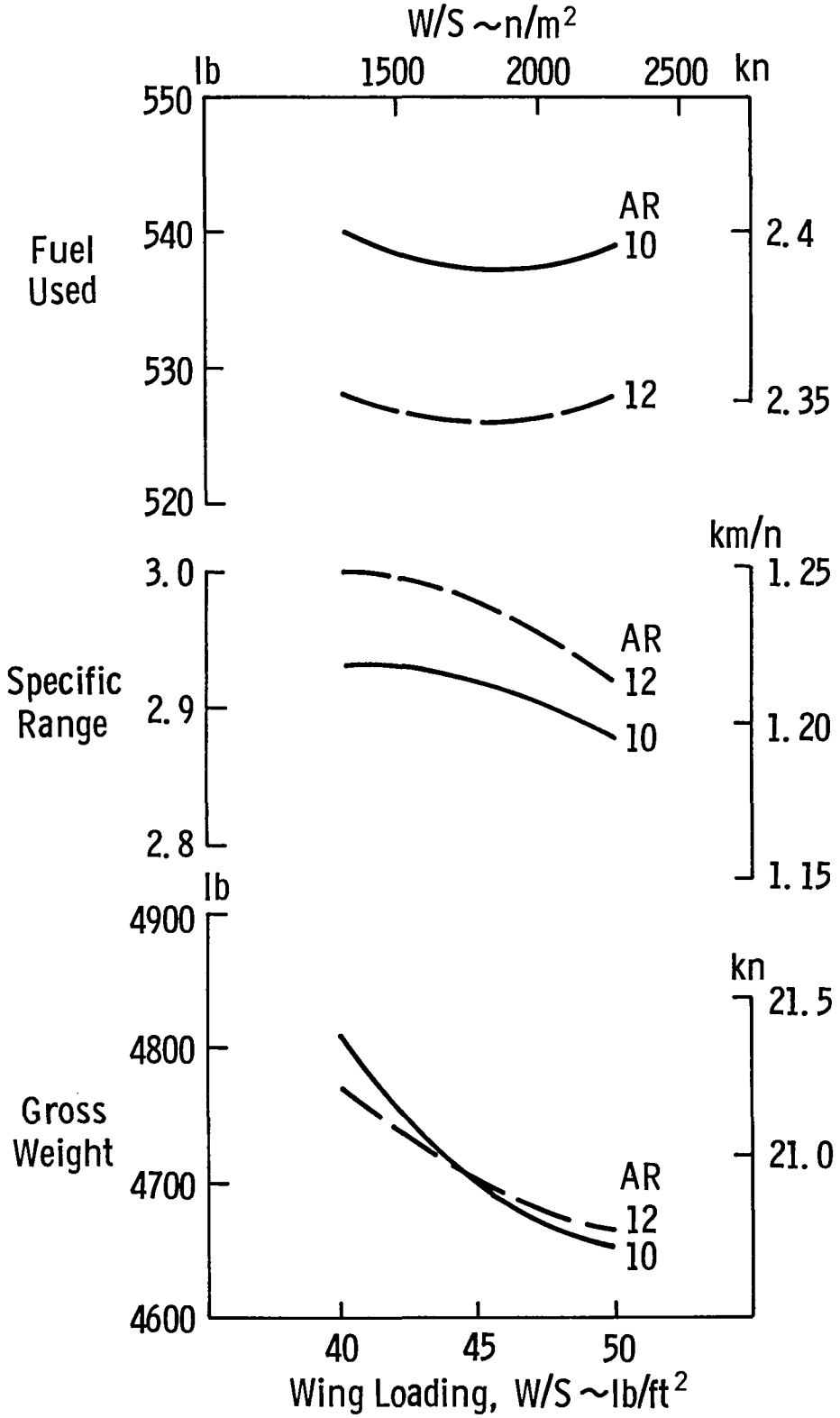

Figure 7.10 Effect of Wing Loading with 350 KT Cruise Speed, Diesel Engine

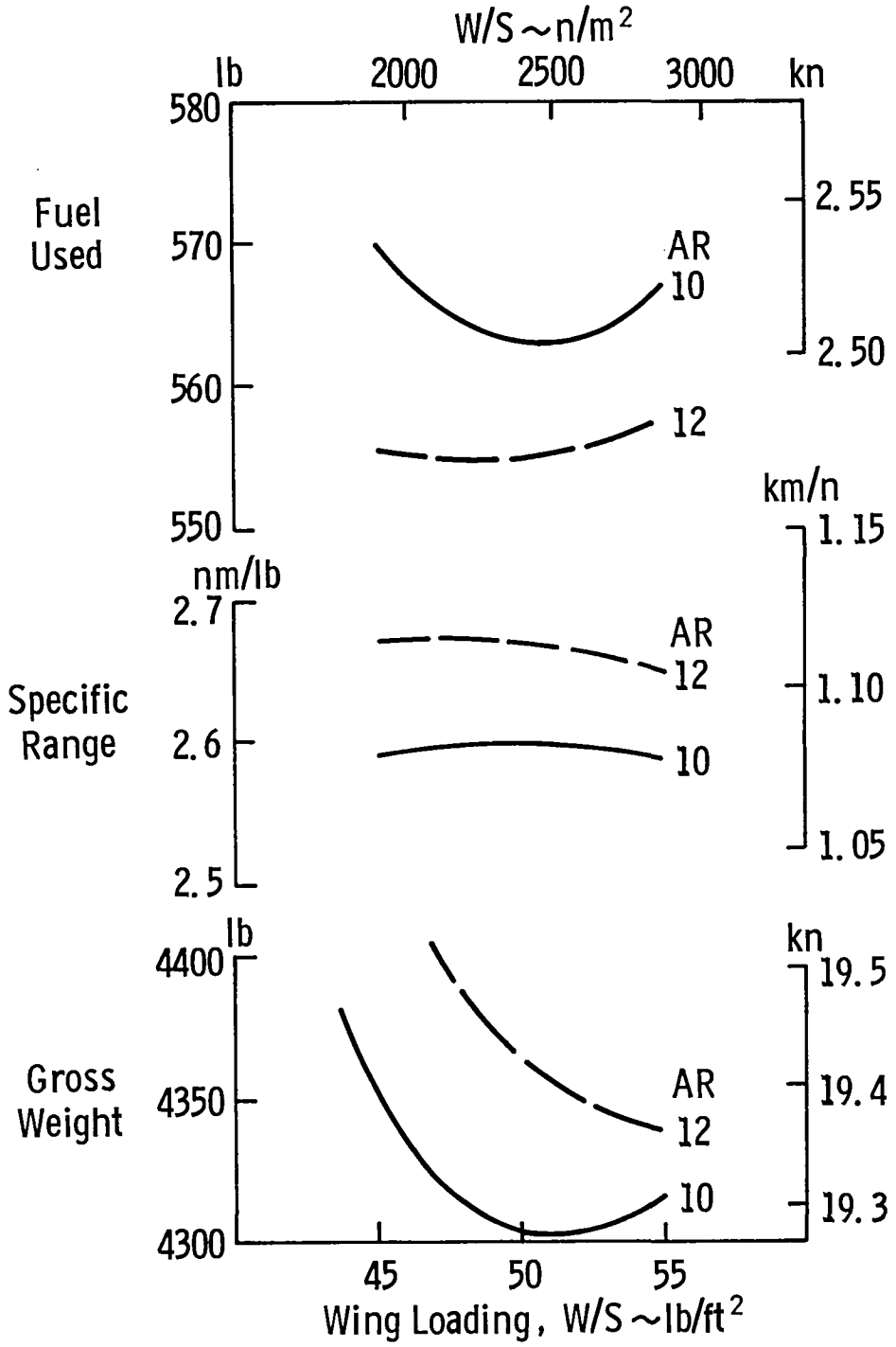

Figure 7.11 Effect of Wing Loading with 350 KT Cruise Speed, Rotary Engine

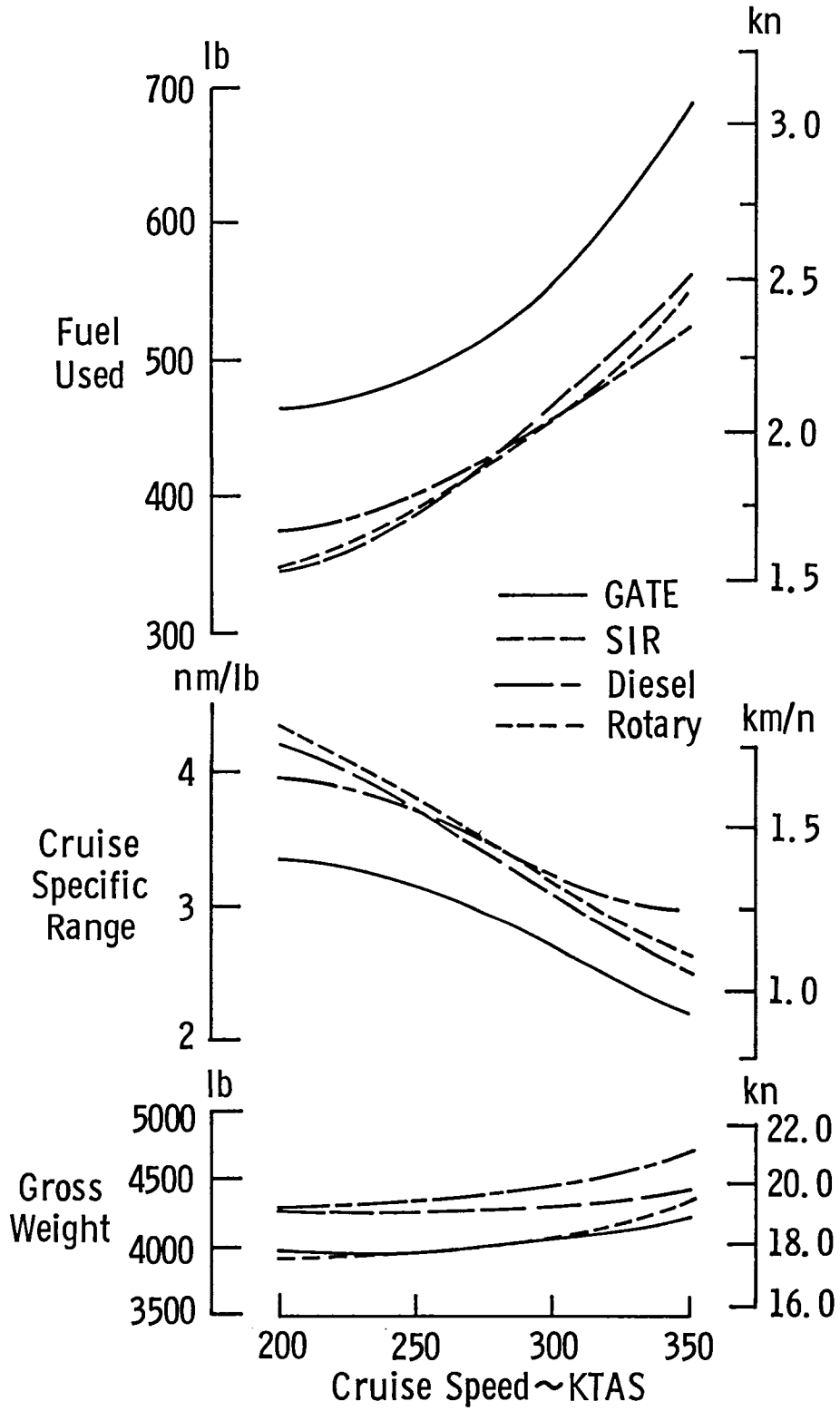

Figure 7.12 Effect of Cruise Speed. Optimum W/S, AR = 12, Pusher Propeller, Laminar Flow Wing and Fuselage

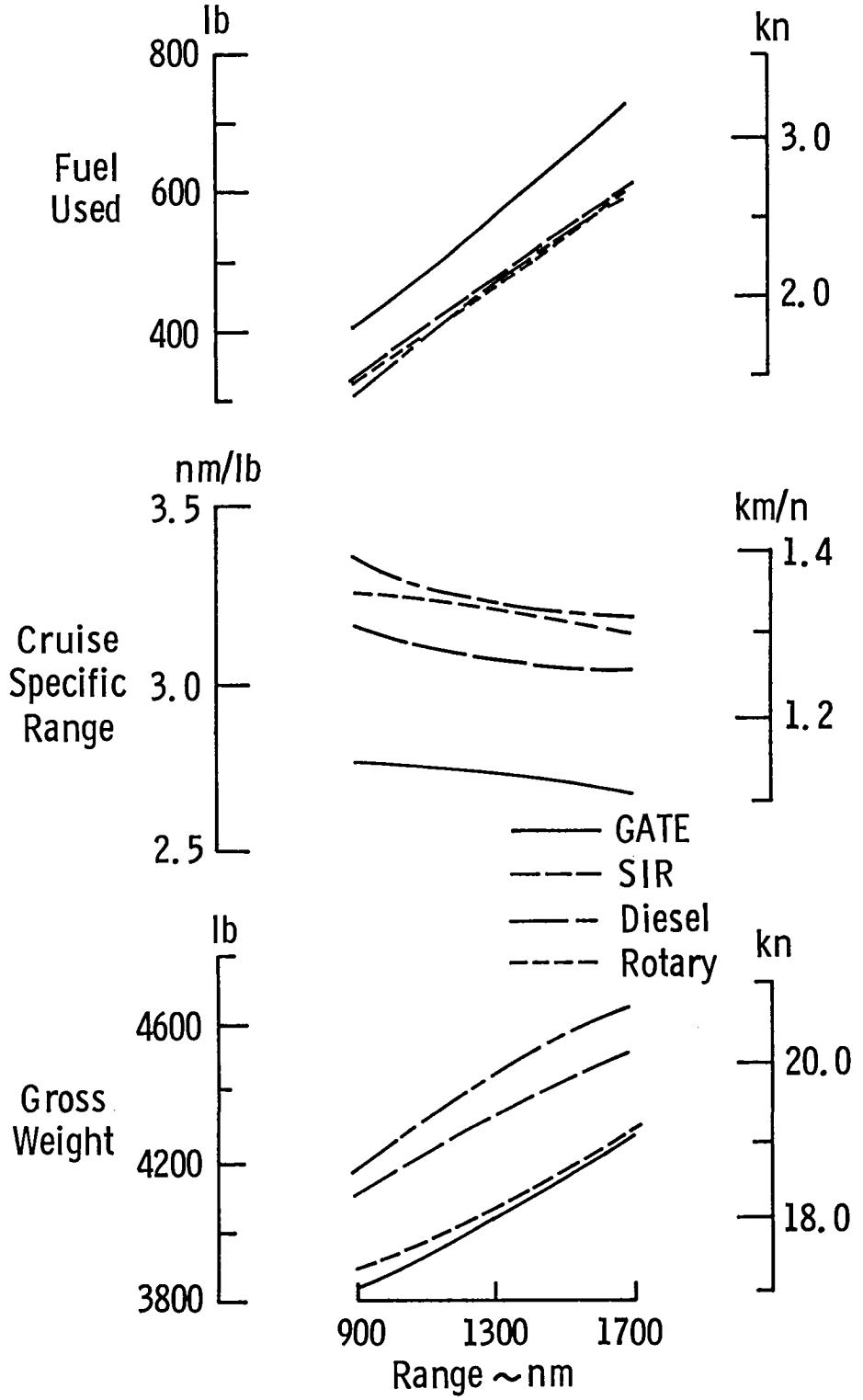

Figure 7.13 Effect of Range. Optimum W/S, AR = 12, Pusher Propeller, Laminar Flow Wing and Fuselage

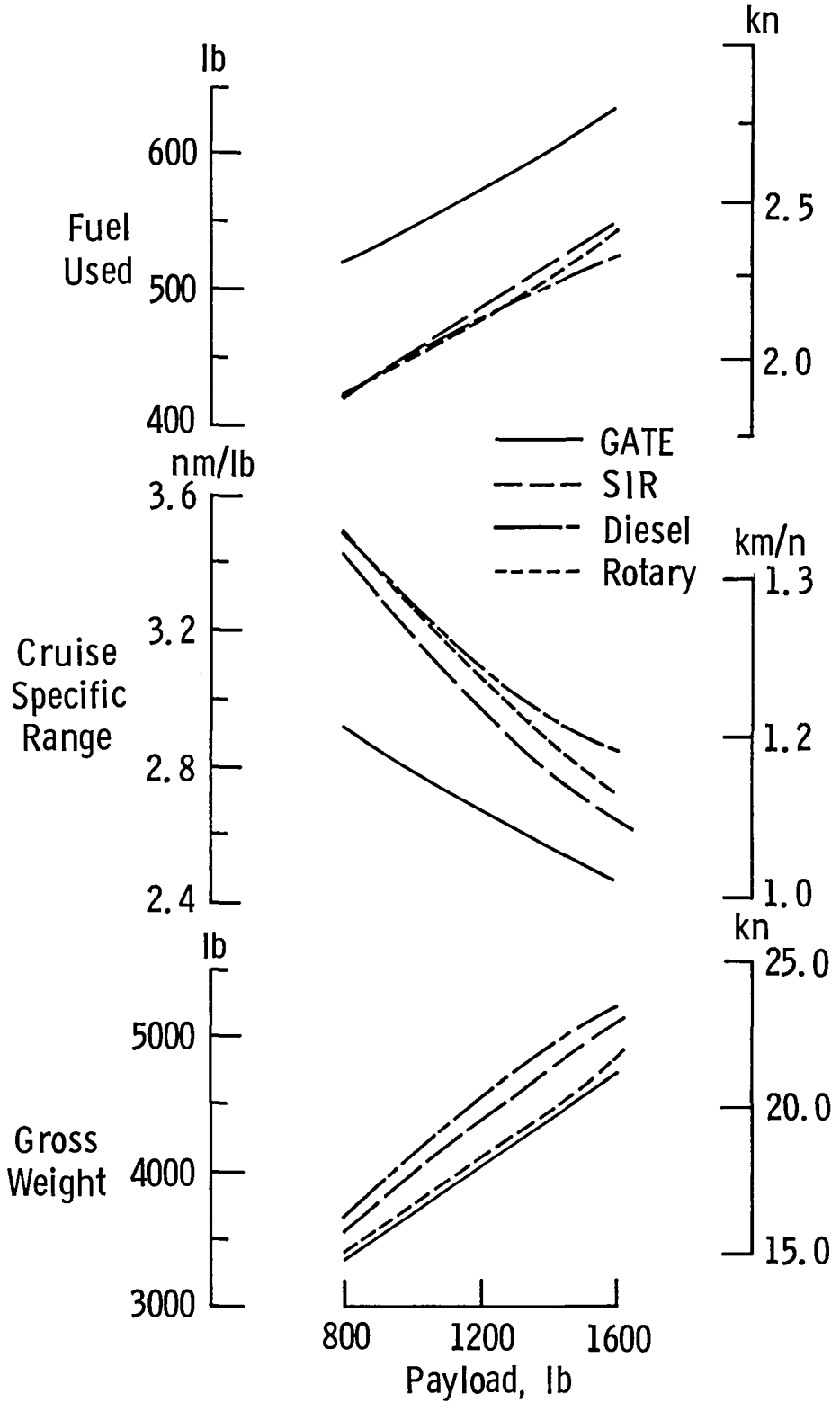

Figure 7.14 Effect of Payload. Optimum W/S, AR = 12, Pusher Propeller, Laminar Flow Wing and Fuselage

8. ADVANCED CONFIGURATIONS

8.1 Composite Airframe

The use of advanced fiber composites can reduce aircraft structural weight considerably, resulting in significant fuel savings.

Composite material systems that have been used in aircraft applications include various epoxy matrices reinforced with fiberglass, graphite fibers, boron fibers, and Kevlar.

Fiberglass/epoxy has been used for primary structure in sailplanes for a number of years. Other applications in FAA certified aircraft include helicopter rotors. The primary advantages of fiberglass composites are that they produce very smooth exterior surfaces; they are resistant to fatigue; they have a high damage tolerance; and they allow relatively easy construction, especially with complex curvatures. The use of fiberglass composites does not normally provide a significant weight advantage over aluminum construction.

Boron/epoxy structures are in service in a number of applications, including 33 experimental F-15 empennages. This material has excellent properties but is still too expensive for most commercial uses.

Kevlar, a synthetic aramid fiber made by DuPont, has a very high specific tensile strength and stiffness but fails at relatively low stress levels in compression. Thus Kevlar composites may be more suited for stiffness-limited components such as fairings and possibly fuselage structures. Kevlar composites have much better impact absorption characteristics than graphite or boron composites. Current appli-

cations include fairings, helicopter fuselages, some control surfaces, and wing leading edges for the Lear Fan aircraft. Kevlar is intermediate in cost between fiberglass and graphite composites.

Graphite/epoxy (Gr/Ep) is the most promising system for primary structure applications in civil aircraft. A number of commercial aircraft components made of graphite/epoxy have been flown for service testing, including Boeing 737 spoilers. The Boeing 757 and 767 will be produced with Gr/Ep control surfaces. The McDonnell-Douglas AV-8B Harrier utilizes a wing made of Gr/Ep. Finally, the LearAvia Lear Fan, an aircraft similar to the baseline for this study, is made almost entirely of Gr/Ep.

Weight savings for Gr/Ep structural designs reported in the literature vary widely, from 20 to 40%. Weight savings for components designed to substitute for the 727 elevator, DC-10 rudder, L-1011 aileron, 737 horizontal stabilizer, DC-10 vertical fin, and L-1011 vertical fin in the NASA Aircraft Energy Efficiency program average 25.7% (Reference 22). The composite (Gr/Ep) forward fuselage structure of the AV-8B is 25.3% lighter than an equivalent metal structure (Reference 23). A comparison of the Lear Fan with the Piper Cheyenne, aircraft performing roughly similar missions, indicates that the structural weight saving for the Lear Fan is about 25%. The Lear Fan is conservatively designed to a +6g limit load factor in order to obtain FAA certification and leave some margin for uncertainties in material properties and environmental effects.

The effects of structural weight reductions of 20, 25, and 30% on the HIPS airplane were investigated using GASP. Table 8.1 presents

the characteristics for these airframes with the advanced diesel engine, compared with the same airframe and engine using conventional structural materials.

The fuselage, wing, and tail structures to which the weight savings are applied make up about 35% of the aircraft empty weight for the advanced diesel airplane, and about 29% of the total gross weight. The reduction in total gross weight is therefore considerably less than the reduction in structural weight.

Questions about the use of composites in primary structure related to moisture absorption, lightning strike protection, crash-worthiness, and manufacturing costs are rapidly being answered. As the technology of manufacturing composite airframes matures, they may become less costly than conventional construction. It is also anticipated that somewhat greater weight savings may be achieved as experience with composites increases.

Table 8.1 Comparison of Conventional Aluminum and Composite Airplanes with Pusher Engines, Laminar Wing, Advanced Diesel Engine -- Baseline Mission Performance

	Wing Loading psf	Aspect Ratio	Gross Weight, lb.	Change in Gross Weight	Fuel Used, lb.	Fuel Saved	Average Cruise Specific Range, nm/lb.	Change in Engine Size
Conventional Structure	50	12	4458	-	461	-	3.21	-
-20% ΔW Composite Airframe	50	12	4144	-7%	444	3.7%	3.32	-4.7%
-25% ΔW Composite	50	12	4061	-8.9%	440	4.6%	3.35	-5.8%
-30% ΔW Composite	50	12	3990	-10.5%	435	5.6%	3.38	-7.4%

8.2 Canard Configuration

Most conventional configurations fly with a down load on the horizontal stabilizer requiring an increase in lift on the main wing. The resulting increased induced drag is the main component of trim drag. The use of a canard configuration, where both control and wing surfaces produce lift, would appear to allow a reduction in trim drag, if there is no change in wing area and span.

The downwash/upwash field from the canard can significantly affect the aft wing. At cruise, with a canard of shorter span than the wing, the inboard main wing section will be in downwash, while the outboard section will experience upwash. Twisting the wing tip sections down relative to the root can help equalize the wing lift distribution, and result in a thrust component sufficient to offset the drag caused by the downwash field.

A canard configuration was analyzed based on a main wing aspect ratio of 12 and a pusher engine. The passenger cabin for the canard design is identical to that of the baseline design. Detailed weight and balance and aerodynamic center calculations were not performed, but minor adjustments in wing location and sweep should produce a viable configuration.

The change in center of gravity location as fuel is burned can be a problem with canard designs if fuel is carried in the wing only. Use of fuselage or wing strake fuel tanks may be necessary. Fuselage fuel tanks can be acceptable from a safety standpoint if measures used in military aircraft and helicopters are adopted, such as nylon reinforced fuel bladders.

Trim change with wing flap deflection may also be a problem if the wing is relatively far aft of the aircraft center of gravity. Minimizing the canard area to wing area ratio alleviates this problem. A canard/wing area ratio of 0.25 was chosen for this design.

A main wing aspect ratio of 12 was chosen for comparison with the advanced baseline. A canard aspect ratio of 8.0 was chosen to keep the canard chord reasonable.

A computer program using the Quasi Vortex Lattice Method of Lan[24] was used to compare induced drag values for the canard and conventional configurations at angles of attack representative of climb and cruise. Reference area for the canard design is the total lifting area (wing area plus canard area). This facilitates the use of GASP to analyze a canard design. Figure 8.1 shows the induced drag values calculated by QVLM as a function of lift coefficient for the two configurations at various angles of attack and Mach numbers. The induced drag of the canard design is considerably higher than that of the conventional design. Assuming that both designs have the same Oswald efficiency factor, the effective aspect ratio for the canard design is 7.9 in cruise.

GASP was not designed to analyze unconventional configurations, but a close approximation to a canard is possible. Using the total lifting area as the reference area, it is necessary to set the horizontal tail size input to a negligible value. Aspect ratio is set to the effective aspect ratio for the total configuration, 7.9. Normal fuselage geometry is used. This results in an airplane with less wetted area due to the shorter fuselage and elimination of the horizontal tail.

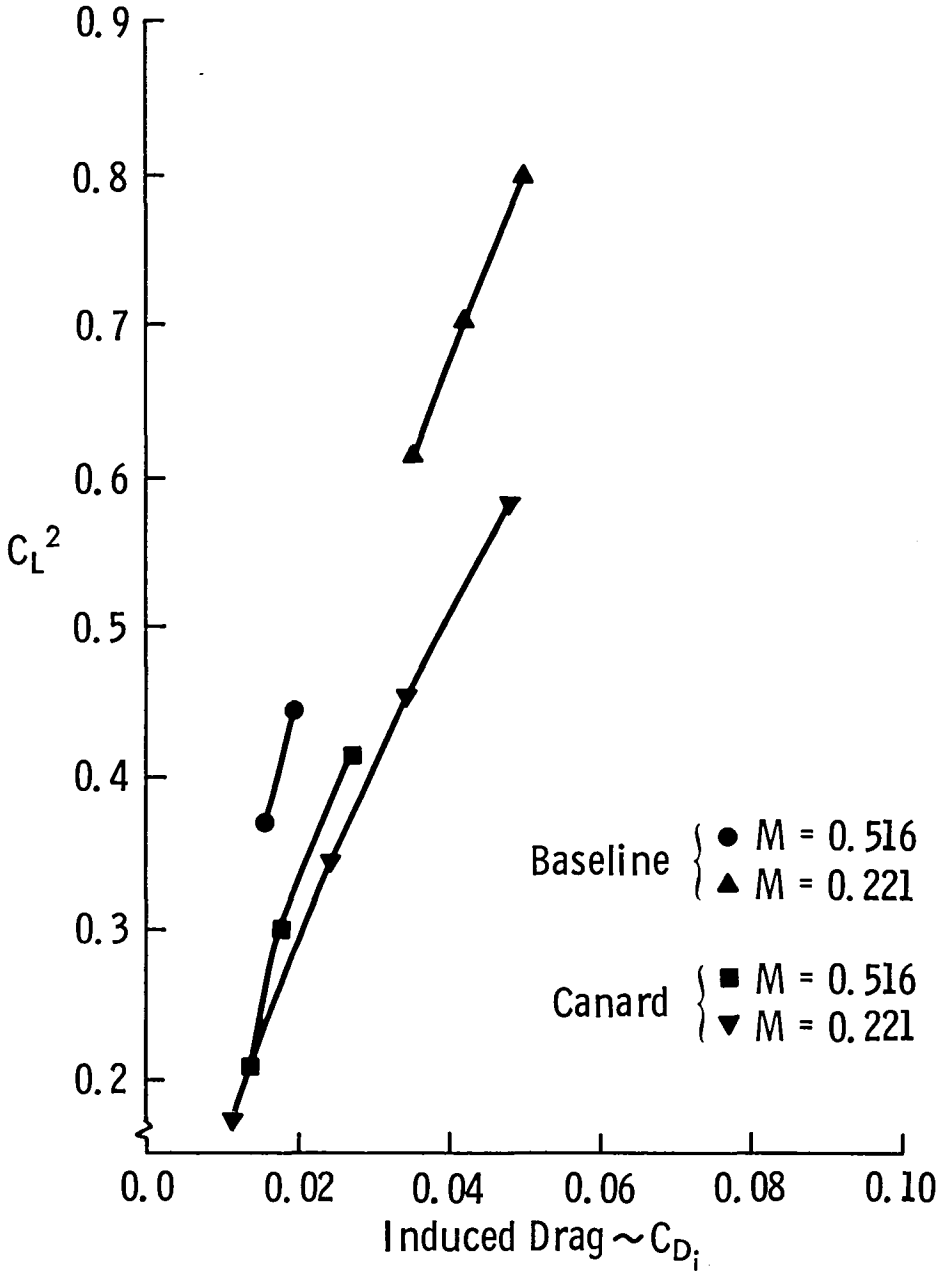

Figure 8.1 Theoretical Prediction of Induced Drag of a Canard and Conventional Airplane Using QVLM Program

Table 8.2 compares the performance of a diesel engine pusher canard design with composite structure to a conventional configuration also utilizing composites.

The differences in wetted areas and fuselage weight more than make up for the less favorable induced drag of the canard design in this case. Improvements in all four categories are achieved with the canard configuration.

The induced drag of the canard design could probably be improved by optimizing the canard location and size relative to the wing. Note also that this method of analysis involves a number of approximations; thus the comparisons are not as accurate as those presented for variations in conventional configurations in this report.

Table 8.2 Comparison of Canard and Conventional Configurations With Diesel Pusher Engine and Composite Structure

	Gross Weight, lb	Specific Range, lb	Fuel Used, lb	Engine Size, hp
Canard	3798	3.49	421	1055
Conventional	4061	3.35	440	1100
Improvement due to canard	6%	4%	4%	4%

9. INTEGRATED DESIGN

In order to determine the maximum potential benefits from the synergistic combination of all advanced technologies considered in this study, an advanced technology configuration with the following characteristics was analyzed:

- rotary engine
- pusher propeller
- laminar wing
- laminar flow on forward fuselage
- composite materials with 25% structural weight reduction
- conventional wing-tail configuration

The results are presented in Table 9.1. Performance and configuration improvements relative to the baseline and current production aircraft are extremely large. The gross weight is 33% less than the baseline airplane (Table 3.3) and the total fuel has been reduced to 43.7% of that used by the baseline airplane.

Figure 9.1 underscores the dramatic advances that are possible in fuel efficiency and performance through the application of advanced technology. The integrated design achieves four times the specific range of current turboprops with comparable speed, or doubles the specific range (and total range) of the best current single-engine piston airplanes while increasing cruise speed by 100 knots.

Table 9.1 Advanced Integrated Configuration Summary. (Pusher Rotary Engine, Laminar Flow, Composite Structure)

Configuration Data:

gross weight	3690 lb_2
wing area	73.8 ft^2
wing loading	50 lb/ft^2
aspect ratio	12
wing fuel volume	72.5 gal
empty weight	2050 lb
maximum payload	1200 lb
engine	Rotary
sea level max. power	581 hp
propulsion system weight	657 lb

Performance:

cruise speed	297.8 kt
cruise altitude	35,000 ft
range (max. payload)	1300 nm
average cruise specific range	3.34 nm/lb
total fuel for max. payload mission	433 lb
range (max. fuel)	1300 nm
takeoff distance to 50 ft	2112 ft
landing distance from 50 ft	1309 ft
stall speed (takeoff, max. gross weight)	76.2 kt
stall speed (landing, max. gross weight)	64.7 kt
stall speed (landing, end of mission)	60.8 kt
L/D_{max}	18.16
L/D_{cruise}	16.13

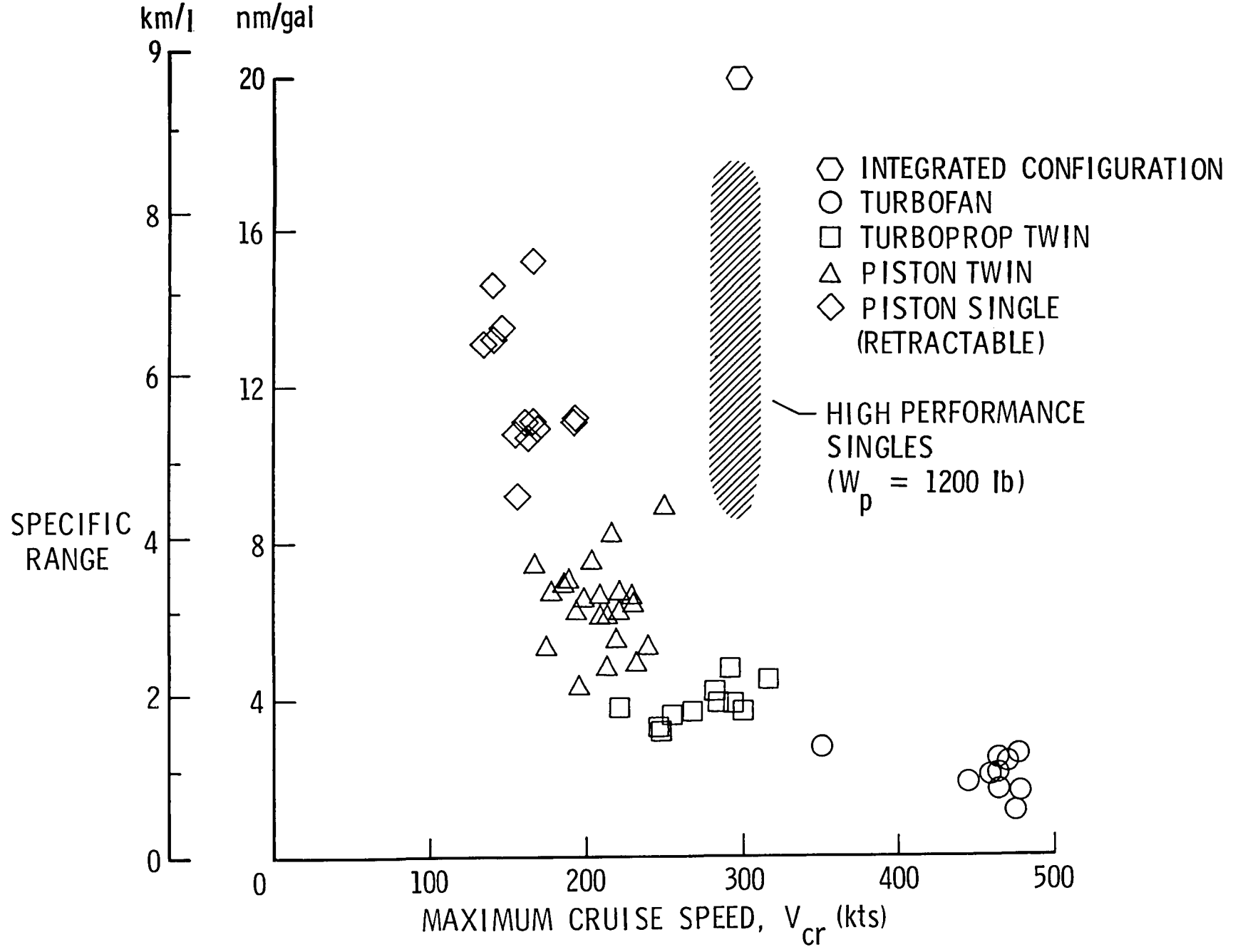

Figure 9.1 Comparison of Specific Range and Cruise Speed for Current and Advanced Technology Airplanes

10. CONCLUSIONS

The potential exists to greatly improve the fuel efficiency and mission capability of single-engine airplanes through the application of advanced technology to engines, aerodynamic design, and materials.

The turbine engine, while being very light weight, cannot match advanced internal combustion engines in fuel economy for this mission. Its relatively high cost may also be a deterring factor.

The other three engines considered have very nearly equal fuel performance, but the rotary engine produces the lightest and smallest airplane. Other attractive features of the rotary are its relatively small size, competitive cost, multifuel capability, and simplicity. The low lapse rate, which results in a low maximum power rating, depends on advancements in the technology of turbochargers. However, the SIR engine has the benefit of tradition, operational experience, and customer acceptance.

To take full advantage of technologies that can reduce fuel consumption, some modification to the FAR rule requiring a stall speed less than 61 knots will be needed.

Laminar flow wings, combined with composite structural materials, offer considerable promise for improved performance and fuel efficiency.

With vigorous development of the technologies discussed herein, significant improvements can be achieved in the performance, efficiency, and utility of general aviation aircraft during the next decade.

REFERENCES

1. Bruce J. Holmes, "Aerodynamic Design Optimizations of a Fuel Efficient High-Performance Single-Engine Business Airplane." AIAA Paper No. 80-1846, 1980.

2. David L. Kohlman, Garey T. Matsuyama, Kevin E. Hawley, and Paul T. Meredith, "A Feasibility Study for Advanced Technology Integration for General Aviation." NASA CR-159381, 1980.

3. T.J. Wickenheiser, G. Knip, R. M. Plencner, and W. C. Strack, "Comparisons of Four Alternative Powerplant Types for Future General Aviation Aircraft." NASA TM-81584, 1980.

4. Bruce J. Holmes and Cynthia C. Croom, "Aerodynamic Design Data for a Cruise-Matched High Performance Single Engine Airplane." SAE Paper No. 810625, 1981.

5. "GASP — General Aviation Synthesis Program." NASA CR-152303, prepared by Aerophysics Research Corp., January 1978.

6. David L. Kohlman, "Flight Test Results for an Advanced Technology Light Airplane." Journal of Aircraft, Vol. 16, April 1979, pp. 250-255.

7. Bruce J. Holmes, "Flight Evaluation of an Advanced Technology Light Twin-Engine Airplane (ATLIT)." NASA CR-2832, July 1977.

8. B.J. Holmes, C. J. Obara, and L. P. Yip, "Natural Laminar Flow Experiments on Modern Airplane Surfaces," NASA TP-2256, 1984.

9. B. J. Holmes, C. J. Obara, G. M. Gregorek, M. J. Hoffman, and R. J. Freuhler, "Flight Investigation of Natural Laminar Flow on the Bellanca Skyrocket II," SAE Paper 830717, April 1983.

10. B. J. Holmes and C. J. Obara, "Observations and Implications of Natural Laminar Flow on Practical Airplane Surfaces." ICAS Paper 82-5.1.1. Presented at the ICAS Meeting, Seattle, August 1982.

11. Dan M. Somers, "Design and Experimental Results for a Natural-Laminar-Flow Airfoil for General Aviation Applications." NASA TP-1861, 1981.

12. D. L. Kohlman, W. G. Schweikhard, and A. E. Albright, "Icing Tunnel Tests of a Glycol-Exuding Porous Leading Edge Ice Protection System on a General Aviation Airfoil." NASA CR-165444, 1981.

13. R. F. Sturgeon et al.: "Evaluation of Laminar Flow Control System Concepts for Subsonic Commercial Transport Aircraft." NASA CR-159253, 1980.

14. J. B. Peterson, and D. F. Fisher, "Flight Investigation of Insect Contamination and Its Alleviation." NASA CP-2036, 1978.

15. "General Aviation Propulsion," Proceedings of NASA Lewis Conference. NASA CP-2126, November 1979.

16. A. P. Brouwer, "150 and 300 KW Lightweight Diesel Aircraft Engine Design Study." NASA CR-3260, 1980.

17. C. Jones and M. Berkowitz, "Multifuel Rotary Aircraft Engine." AIAA Paper 80-1237, June 1980.

18. A. D. Galbraith, "Electric Propulsion for High-Performance Aircraft." AIAA Paper No. 79-1265, June 1979.

19. USAF Stability and Control Datcom. Contracts AF 33(616)-6460 and F33615-75-C-3067, McDonnell Douglas Corp., October 1960. (Revised April 1976).

20. Flying Annual and Buyer's Guide, Ziff-Davis, 1978.

21. K. L. Sanders, SAWE Paper 761, SAWE Journal, May 1961.

22. Louis F. Vosteen, "Composite Aircraft Structures", in "Fibrous Composites in Aircraft Design," proceedings of the Fourth Conference on Fibrous Composites, San Diego, 1978.

23. James C. Watson, "AV-8B Composite Fuselage Design." J. of Aircraft, Vol. 19, No. 3, March 1982, pp. 235-238.

24. C. E. Lan, "A Quasi-Vortex-Lattice Method in Thin Wing Theory," Journal of Aircraft, Vol. 11, No. 9, Sept. 1974, pp. 518-527.

1. Report No.	2. Government Accession No.	3. Recipient's Catalog No.
NASA CR-3863		

4. Title and Subtitle	5. Report Date
DESIGN STUDY OF TECHNOLOGY REQUIREMENTS FOR HIGH PERFORMANCE SINGLE-PROPELLER-DRIVEN BUSINESS AIRPLANES	January 1985
	6. Performing Organization Code
7. Author(s) *David L. Kohlman and James Hammer*	8. Performing Organization Report No. KU-FRL-487-1
	10. Work Unit No.
9. Performing Organization Name and Address *Flight Research Laboratory* *University of Kansas Center for Research, Inc.* *Lawrence, KS 66045*	11. Contract or Grant No. *NAS1-16363*
	13. Type of Report and Period Covered *Contractor Report*
12. Sponsoring Agency Name and Address *National Aeronautics and Space Administration* *Washington, DC 20546*	14. Sponsoring Agency Code 505-45-43-02

15. Supplementary Notes

Langley Technical Monitor: Bruce J. Holmes
Final Report

16. Abstract

Recent developments in aerodynamic, structural and propulsion technologies have greatly influenced the potential for significant improvements in both performance and fuel efficiency of general aviation business airplanes. These advancements include such technologies as natural laminar flow, composite materials, and advanced intermittent combustion engines. The design goal chosen for this parameter design study is a range of 1300 nm at 300 knots true airspeed with a payload of 1200 lbs at 35,000 ft cruise altitude. The purpose of this study is to identify the individual and synergistic effects of various advanced technologies on the optimization of this class of high-performance, single-engine, propeller-driven business airplanes.

17. Key Words (Suggested by Author(s))	18. Distribution Statement
General Aviation *Business Aircraft* *Performance* *Aerodynamics* *Propulsion*	*Unclassified - Unlimited* *Subject Category 02*

19. Security Classif. (of this report)	20. Security Classif. (of this page)	21. No. of Pages	22. Price
Unclassified	*Unclassified*	104	A06

For sale by the National Technical Information Service, Springfield, Virginia 22161

NASA-Langley, 1985